Palaeogeography, Palaeoclimatology, Palaeoecology 458 (2016) 118–132

Contents lists available at ScienceDirect

Palaeogeography, Palaeoclimatology, Palaeoecology

journal homepage: www.elsevier.com/locate/palaeo

Middle–Late Ordovician (Darriwilian–Sandbian) decoupling of global sulfur and carbon cycles: Isotopic evidence from eastern and southern Laurentia

Seth A. Young [a,*], Benjamin C. Gill [b], Cole T. Edwards [c], Matthew R. Saltzman [d], Stephen A. Leslie [e]

[a] Department of Earth, Ocean & Atmospheric Science, Florida State University, Tallahassee, FL 32306, United States
[b] Department of Geosciences, Virginia Polytechnic Institute & University, Blacksburg, VA 24061, United States
[c] Department of Earth and Planetary Sciences, Washington University, Saint Louis, MO 63130, United States
[d] School of Earth Sciences, The Ohio State University, Columbus, OH 43210, United States
[e] Department of Geology and Environmental Science, James Madison University, Harrisonburg, VA 22807, United States

ARTICLE INFO

Article history:
Received 15 June 2015
Received in revised form 15 September 2015
Accepted 21 September 2015
Available online 8 October 2015

Keywords:
Sulfur isotopes
Carbon isotopes
Pyrite burial
Oxygenation
Weathering
Ordovician

ABSTRACT

Middle–Late Ordovician sequences from the Appalachian Basin and Arbuckle Mountain regions of North America were analyzed for carbonate-associated sulfate ($\delta^{34}S_{CAS}$) and pyrite ($\delta^{34}S_{pyr}$) paired with carbonate ($\delta^{13}C_{carb}$) and organic matter ($\delta^{13}C_{org}$) chemostratigraphy. Two major negative drops in $\delta^{34}S_{CAS}$ (12‰ excursions) are recognized: the older decline in $\delta^{34}S_{CAS}$ occurs within the *Histiodella holodentata–Phragmodus polonicus* Conodont Zones and the younger drop is within the *Cahabagnathus sweeti–Amorphognathus tvaerensis* (*Baltoniodus gerdae* subzone) Zones. These overall these negative shifts in $\delta^{34}S_{CAS}$ have an antithetical relationship with positive shifts in $\delta^{34}S_{pyr}$ (~+10‰) and $\delta^{13}C_{carb}$ (~+2‰) recorded in the same successions. The older negative $\delta^{34}S_{CAS}$ shift is coincident with the widely documented mid-Darriwilian $\delta^{13}C$ excursion (MDICE), and the younger negative $\delta^{34}S_{CAS}$ shift is coincident with another positive $\delta^{13}C_{carb}$ shift in the early Sandbian. Geochemical modeling of these sulfur isotope shifts suggests that a decrease in the global rate of pyrite burial or isotope fractionation between seawater sulfate and sedimentary pyrite could account for these negative $\delta^{34}S_{CAS}$ trends. Additionally, a substantial increase in the weathering flux of pyrite to the global oceans could also explain these secular sulfur isotope trends. While increased crustal weathering is broadly consistent with a sea-level lowstand, and the seawater $^{87}Sr/^{86}Sr$ isotope record of change in continental weathering in the late Darriwilian Stage of the Ordovician, geologic and geochemical proxy evidence do not support distinct pulses of continental weathering required to generate two separate negative shifts in $\delta^{34}S_{CAS}$. These antithetical isotope trends may be best explained by changes in the marine redox state that significantly reduced microbially mediated pyrite burial and organic matter remineralization rates. Pulses of oceanic ventilation would have expanded habitable environments for marine organisms, and thus is broadly consistent with major increases in biodiversification during this period of the Ordovician.

1. Introduction

The Great Ordovician Biodiversification Event (GOBE) is widely acknowledged to be one of two major components of the profound radiation of animal life in the Early Paleozoic, the other being the Cambrian Explosion (Sepkoski et al., 1981; Droser et al., 1997; Sheehan, 2001; Webby et al., 2004). This significant and continuous rise in the biodiversity and biocomplexity of marine organisms occurred throughout the Early and Middle Ordovician (~25–30 m.y. interval) with the largest surges within the Early Dapingian and Mid-Darriwilian global stages (Droser and Finnegan, 2003; Harper, 2006; Zhan and Harper, 2006; Rasmussen et al., 2007; Servais et al., 2008, 2010). Several hypotheses have been put forward for the GOBE. Climatic cooling throughout the Early Ordovician has been proposed as a cause of the GOBE (Trotter et al., 2008) where sea surface temperatures declined creating global climatic conditions favorable for diversification of marine life. Alternatively, L-chondrite asteroid breakup, tectonic events, sea-level, nutrient availability, and global climate state changes have also been linked to Ordovician biodiversification (Miller and Mao, 1995; Achab and Paris, 2007; Schmitz et al., 2008; Cardenas and Harries, 2010). Furthermore these environmental and biological changes have also been linked to a possible mantle superplume event (Barnes, 2004). With these diverse ranges of causal mechanisms proposed for the GOBE, it remains challenging to single out any one environmental factor to completely explain this diachronous and multifaceted evolutionary event.

Geochemical records, primarily $\delta^{34}S$ and $\delta^{13}C$, of Late Neoproterozoic (Ediacaran Period) sedimentary sequences have revealed ocean–

* Corresponding author.
E-mail address: sayoung2@fsu.edu (S.A. Young).

http://dx.doi.org/10.1016/j.palaeo.2015.09.040
0031-0182/

atmosphere oxygenation events that are linked to critical appearance and diversification events of marine life (Fike et al., 2006; Canfield et al., 2007; Halverson and Hurtgen, 2007). However, it appears that these pulses of oxygen may have had only regional–local scale influences on marine environments as other isotopic studies suggest that widespread deep-ocean anoxia and sulfidic (euxinic) conditions persisted from the Ediacaran throughout much of the Cambrian (Hough et al., 2006; Canfield et al., 2008; Hurtgen et al., 2009; Ries et al., 2009; Li et al., 2010; Sperling et al., 2015). Late Cambrian studies focused the widely documented Steptoean Positive Carbon Isotope Excursion or SPICE — a +4–6‰ shift in $\delta^{13}C_{carb}$ representing a global perturbation of the carbon cycle (Saltzman et al., 2000, 2004) — have documented large, synchronous positive shifts in both carbonate-associated sulfate and pyrite ($\delta^{34}S_{CAS}$ and $\delta^{34}S_{pyr}$). This pattern suggests widespread euxinic conditions in the oceans during the SPICE (Hurtgen et al., 2009; Gill et al., 2011a, 2011b). A companion study focused on oxygen production associated with the organic carbon and pyrite burial event during the SPICE and suggested that atmospheric O_2 increased ~10–18% in the wake of the SPICE (Saltzman et al., 2011). Further, Saltzman et al. (2011) linked this oxygenation event to a time of major plankton diversification (Servais et al., 2008) initiating a critical step in the Paleozoic food web necessary for the GOBE. However, as with the Neoproterozoic oxygenation events, it is possible that much of this oxygen produced by the SPICE was consumed by oxidation of reduced species in oceans or on land since evidence for anoxia appears to persist into the Ordovician (Pruss et al., 2010; Thompson and Kah, 2012; Saltzman et al., 2015). Here we present a carbon and sulfur isotope study of the Middle–Late Ordovician to investigate the potential links between ocean and atmosphere redox and the GOBE.

Sulfur, a major chemical element required by organisms on Earth, is dynamically cycled between organic substrates and abiotic reservoirs through reduction/oxidation reactions that proceed both abiotically and by biological catalysis. The long-term carbon and sulfur cycles are coupled through oxidation of biomass produced largely from oxygenic photosynthesizers during the anaerobic process of microbial sulfate reduction (MSR) (e.g., Berner, 2004 and references therein). Marine sulfate levels are intrinsically linked to atmospheric O_2 levels because the predominant flux of sulfate to the oceans is through oxidative weathering on land of pyrite and other sulfide minerals. Microbial sulfate reducers produce hydrogen sulfide (H_2S) during their metabolism and, in the presence of dissolved Fe^{2+}, sulfide minerals like pyrite (FeS_2) are rapidly (hours to 10 s of years, depending upon Fe-bearing minerals present) precipitated (e.g., Canfield et al., 1992). In modern ocean settings MSR primarily occurs in the sediments, however when it occurs in the water column biological stress often is observed because H_2S is toxic to most aerobic organisms (Garrels and Lerman, 1981; Murray, 1995; Lenton and Watson, 2000). Coupled sulfur and carbon isotopic analyses provide the possibility to document past fluctuations in the carbon and sulfur cycles and in turn give us unique insights into oceanic–atmospheric redox evolution.

To date geochemical investigations of strata spanning this major Ordovician biotic transition have primarily focused on the carbon cycle ($\delta^{13}C$ records; Buggisch et al., 2003; Saltzman, 2005; Munnecke et al., 2011; Edwards and Saltzman, 2014, 2016), with only two studies focused on the sulfur cycle (combined $\delta^{34}S_{CAS}$ and $\delta^{13}C_{carb}$ records; Thompson and Kah, 2012; Marenco et al., 2013). Presented here carbonate-associated sulfate and pyrite ($\delta^{34}S_{CAS}$ and $\delta^{34}S_{pyr}$) records along side of carbonate and organic carbon records ($\delta^{13}C_{carb}$ and $\delta^{13}C_{org}$) from two Middle to Late Ordovician (Late Dapingian to Early Sandbian Stage) sequences from widely separated basins in North America (Fig. 1). The sulfur and carbon isotopic data, $\Delta^{34}S$ trends ($\delta^{34}S_{CAS}$–$\delta^{34}S_{pyr}$) are evaluated alongside previously published data (Thompson and Kah, 2012) and examined with box model simulations to explore global rates of pyrite burial/weathering, chemocline migration within the sediments, and the redox state of the global oceans in the Middle–Late Ordovician. Our results reveal potential connections of the progressive ventilation of marine environments to the widely recognized major pulses of biodiversity during the GOBE.

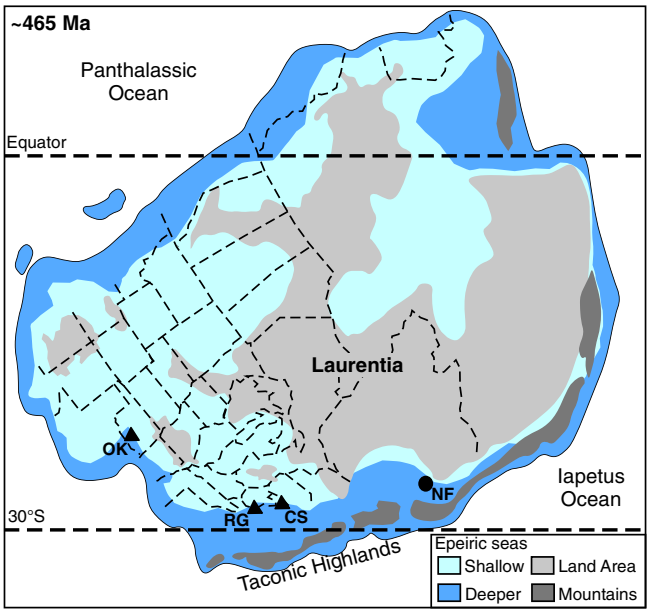

Fig. 1. Middle Ordovician paleogeographic map (modified from Ron Blakey: http://jan.ucc.nau.edu/~rcb7/globaltext.html) with locations of the study areas (triangles) near Clear Spring, Maryland and Arbuckle Mountains, Oklahoma shown. A previously studied Darriwilian section (circle) from Western Newfoundland is also shown (Thompson and Kah, 2012).

2. Geologic setting

2.1. Depositional environments, facies, and sequence stratigraphy

Middle Ordovician carbonates from the Central Appalachians were deposited on a shallow marine platform on the southern margin of the paleocontinent of Laurentia, and contain a well-documented hiatus known as the Knox Unconformity (e.g., Mussman and Read, 1986). This disconformity commonly marks the transition from passive margin shelf deposits to active margin deposition in a foreland basin associated with the Taconic orogeny and the duration of time it represents varies across the Appalachians (Repetski and Harris, 1986; Leslie et al., 2011; Read and Repetski, 2012). Our study includes a stratigraphic section well exposed along Interstate-70 near Clear Spring, Maryland where this major hiatus is not recognized (Brezinski et al., 1999). Here a practically complete Dapingian to Early Sandbian sequence includes the upper Rockdale Run Formation, Pinesburg Station Dolomite, St. Paul Group (Row Park and New Market Formations), and Chambersburg Formation (Brezinski, 1996; Brezinski et al., 2012).

The Rockdale Run Formation at the base of the sequence at Clear Spring is predominantly a lime mudstone, and with the overlying thin-medium bedded dolostones of the Pinesburg Station Dolomite, represent restricted tidal flat environments (Brezinski et al., 2012). The overlying Row Park Formation contains predominantly fenestral lime mudstones and minor mud-cracked wackestone/dolostones. These with stromatolitic limestone beds at the base of New Market Formation are interpreted to represent peritidal to subtidal carbonate platform environments (Mitchell, 1985). The increasing abundance of fossiliferous wackestone and packstone beds in overlying upper New Market and Chambersburg Formations reflect a relative sea-level rise/deepening of the basin and a transition to more open marine conditions.

The Arbuckle Mountains region of Oklahoma exposes a thick and mostly complete succession (~700 m) of Middle to Upper Ordovician

shallow marine sedimentary strata (Ham, 1969). The Simpson Group (Joins, Oil Creek, McLish, Tulip Creek, and Bromide Formations) is a mixed siliciclastic and carbonate sequence deposited in a carbonate ramp setting alongside the Southern Oklahoma Embayment (e.g., Hoffman et al., 1974). Our study focuses on outcrop exposures of Darriwilian to Sandbian Oil Creek, McLish, Tulip Creek, and Bromide Formations along Interstate-35 in South–Central Oklahoma (Bauer, 1987; Edwards and Saltzman, 2016).

In the I-35 exposures, the basal quartz arenite and sandy carbonate unit of the Oil Creek Formation are overlain by a thick package of interbedded shales and lime mudstones/wackestone representing a large transgressive–regressive cycle (Lewis, 1982). The overlying McLish Formation records another rise in sea-level, with a basal transgressive shoreface sandstone unit (calcite cemented quartz arenite) overlain by nearshore–distal marine ramp carbonates and shales. The shallow water carbonates of the upper McLish Formation represent a relative shallowing of the basin/sea-level fall (Bauer, 1990). Succeeding this in the basal Tulip Creek Formation, a thick transgressive sandstone unit is overlain by a sequence of shallow marine shelf packstone/grainstones. Above this the relatively thick sandstone and mudstone facies of the lower Bromide Formation interpreted to be of lower shoreface depositional environment and are subsequently overlain by open marine carbonates and shales that represent further deepening of the basin/sea-level rise (Bauer, 1990). The uppermost lime mudstones and wackestones of the Bromide Formation (Pooleville Member) represent a restricted lagoon, environment and relative fall in sea-level.

2.2. Stratigraphic correlation

Biostratigraphic correlation of Ordovician shallow marine sequences is primarily done using conodonts, as they are abundant in both carbonate platform and continental shelf/slope settings (Cooper and Sadler, 2012). The Clear Spring and the composite Arbuckle Mountains sections have been the subject of detailed conodont biostratigraphic studies, yielding 10–11 conodont zones and placing these strata within the Dapingian through Sandbian global stages of the Ordovician (Boger, 1976; Bauer, 1987, 1990, 2010; Brezinski et al., 1999; Leslie et al., 2013; Saltzman et al., 2014). In these two study areas the following Middle–Upper Ordovician North American Midcontinent conodont zones can be recognized (in ascending order), the *Neomultioistodus compressus–Tricladiodus clypeus*, *Histiodella altifrons*, *Histiodella sinuosa*, *Histiodella holodentata*, *Phragmodus polonicus*, *Cahabagnathus friendsvillensis*, *Cahabagnathus sweeti*, *Plectodina aculeata*, *Erismodus quadridactylus*, and *Belodina compressa* Zones (Webby et al., 2004; Cooper and Sadler, 2012). Several North Atlantic conodont zones can also be recognized (in ascending order), the *Pygodus serra, Pygodus anserinus,* and *Baltoniodus variabilis* and *Baltoniodus gerdae* subzones of the *Amorphognathus tvaernsis* Zone.

Additionally, Sr Isotope Stratigraphy (SIS) was recently used as an additional means of correlation in both of these sequences (Saltzman et al., 2014; Edwards et al., 2015). SIS can be used as a means of global correlation when $^{87}Sr/^{86}Sr$ secular curves are calibrated against biostratigraphy and geochronology (e.g., Ingram et al., 1994; Jones et al., 1994; Jones and Jenkyns, 2001; McArthur et al., 2001). The Ordovician seawater $^{87}Sr/^{86}Sr$ curve has been well documented with $^{87}Sr/^{86}Sr$ values ~0.7090 in the Tremadocian falling to ~0.7078 in the Katian (Denison et al., 1998; Qing et al., 1998), and the highest $^{87}Sr/^{86}Sr$ rates of change (5.0×10^{-5} to 10.0×10^{-5}/m.y.) within the Darriwilian through Sandbian stages (Shields et al., 2003; Young et al., 2009). When rates of $^{87}Sr/^{86}Sr$ change are high ($>5.0 \times 10^{-5}$/m.y.) SIS resolution can be beyond 0.1 m.y. (McArthur et al., 2012). A recent calibration of the Ordovician seawater $^{87}Sr/^{86}Sr$ curve with conodont biostratigraphy and geochronology found a maximum resolution of SIS at ~0.5 to 1.0 m.y. in the Darriwilian and Sandbian (Saltzman et al., 2014).

3. Methods

3.1. Sample preparation and extraction

Following field collections of carbonate samples, a water-based diamond-blade saw was used to remove weathered surfaces and secondary veins. A fraction of the samples was further slabbed and polished to produce thin-section billets for carbon isotope analyses. Thin-section billets and the remaining sample fractions were thoroughly cleaned by ultrasonic bath containing ultrapure (deionized, 18 MΩ) water to remove surficial contaminants. Least altered components (following petrographic examination) were then preferentially micro-drilled (~1 mg for $\delta^{13}C_{carb}$ and ~1 g for $\delta^{13}C_{org}$) from thin-section billets. Sample powders were prepared for $\delta^{13}C_{org}$ analysis, by acidifying ~1 g with 6 N HCl to remove carbonate minerals. Insoluble residues were then repeatedly rinsed in ultrapure water, centrifuged, and dried overnight at 80 °C. The dried residues were homogenized, weighed, and loaded into tin cups for $\delta^{13}C_{org}$ analysis.

The remaining sample fractions (~50–100 g) were then powdered/homogenized using a SPEX 8510 Shatterbox in alumina ceramic containers for CAS and pyrite sulfur analyses. CAS extractions were carried out on each sample using approximately 60 g of powdered rock, using a protocol modified after Burdett et al. (1989), Gill et al. (2007), and Jones and Fike (2013). Sample powders were first soaked in a 10% NaCl solution under constant agitation for 24 h, and subsequently rinsed and agitated in ultrapure water three times to remove any water-soluble sulfate (each water rinse was ~24 h). We then treated samples in a 4% NaOCl solution for 48 h to remove any metastable sulfides and organically bound sulfur. Samples were then subjected to three more ultrapure water rinses (described above) before being acidified using 6 N HCl for 3 h to dissolve $CaCO_3$ and liberate sulfate from the carbonate matrix. The acidified solution was then separated from the insoluble sample residues via centrifugation and the residues were set aside for pyrite sulfur extraction. Acidified solutions were brought to pH ~ 3 and a saturated solution of $BaCl_2$ was added to precipitate dissolved CAS as $BaSO_4$. The $BaSO_4$ was rinsed and centrifuged multiple times with ultrapure water to remove chlorine, and then dried overnight at 80 °C prior to isotopic analysis. Pyrite sulfur was extracted from the remaining acid-insoluble residues using modified protocols described by Canfield et al. (1986), Bruchert and Pratt (1996), and Lefticariu et al. (2006). Briefly, insoluble residues were reacted with a mixture of ~40 ml of 12 N HCl and ~40 ml of 1.0 M chromium chloride ($CrCl_2 \cdot 6H_2O$) in a N_2-purged extraction flask. Flowing N_2 carried evolved H_2S, from FeS_2 decomposition, through a buffer solution (0.1 M citrate solution adjusted to pH 4) into a 0.1 M $AgNO_3$ solution where it was precipitated as Ag_2S. The Ag_2S precipitate is then filtered, rinsed, and dried onto a baked 0.22 μm quartz-fiber filter that is saved for isotopic analyses.

3.2. Isotopic analysis

Homogenized $BaSO_4$ and Ag_2S powders were loaded into tin capsules with excess V_2O_5 and analyzed for their $\delta^{34}S$ content by SO_2-method using a Costech Elemental Analyzer coupled to a Thermo Finnigan Delta V isotope ratio mass spectrometer via a Conflo IV split interface. Calibration of our samples via SO_2-method was done based on laboratory standards calibrated relative to the IAEA S-1 standard ($\delta^{34}S$, −0.30‰) and NBS-127 ($\delta^{34}S$, +20.3‰). Analytical reproducibility was better than ±0.2‰ for standards and duplicate samples all of which were analyzed in the Stable Isotope Research Facility (SIRF) at Indiana University.

Sample powders for $\delta^{13}C_{carb}$ analyses were first weighed and roasted in a vacuum oven at 100 °C for 8 h to remove water and volatile organic compounds. Then, 100–300 μg of carbonates were reacted at 72 °C with 3–5 drops of anhydrous phosphoric acid for at least 2 h. Stable isotope values were obtained using a Thermo Finnigan Gas Bench II carbonate preparation device directly coupled to an inlet of a Thermo Finnigan

Delta Plus XP isotope ratio mass spectrometer at the SIRF at Indiana University. Isotope ratios were corrected for acid fractionation and ^{17}O contribution and reported in delta notation relative to the V-PDB (‰ Vienna Peedee Belemnite) standard. Precision and calibration of data are monitored through routine analysis of the IAEA NBS-19 standard. Standard deviations for $\delta^{13}C$ and $\delta^{18}O$ are 0.05‰ and 0.10‰, respectively (one sigma).

Stable $\delta^{13}C_{org}$ values were obtained using a Costech Elemental Analyzer coupled to a Thermo Finnigan Delta Plus XP through an open-split Conflo III in the SIRF at Indiana University. Samples are dropped under helium into an oxidation furnace packed with chromium(VI) oxide and silvered cobaltic/cobaltous oxide (to remove any halogens) at 1000 °C. The gas is then passed through a reduction furnace packed with elemental copper at 680 °C to reduce all nitrogen bearing compounds to gaseous nitrogen. The resulting gases are then passed through a water trap to eliminate moisture. Carbon isotope ratios are corrected for ^{17}O contribution and reported in delta notation relative VPDB. Precision and calibration of data are monitored through routine analyses of in-house standards that are calibrated against IAEA standards. Standard deviations for $\delta^{13}C$ are ±0.06‰ (one sigma), and ±0.7% for %C (one sigma). Weight percent of total organic carbon (TOC) in samples is determined by comparison of voltages for the ion beam intensities of masses 44, 45, and 46 CO_2^+ between our samples and known wt.% carbon of the gravimetric standard acetanilide, the uncertainty is better than ±5% (e.g., Young et al., 2008).

4. Results

4.1. Clear Spring, Maryland

Outcrops of the upper Beekmantown Group, St. Paul Group, and lower Chambersburg Formation were sampled continuously at exposures along the westbound lane of I-70 near the town of Clear Spring. Values of $\delta^{34}S_{CAS}$ from the Rockdale Run and Pinesburg Station Dolomite show a significant fluctuation (~7‰ variability) with average values ~+28 to +32‰ with paired $\delta^{34}S_{pyr}$ values increasing roughly from +5‰ to +12‰ (Fig. 2). In the upper Pinesburg Station Dolomite through lower Row Park Formation $\delta^{34}S_{CAS}$ values sharply decline from values at +35‰ to +23‰, while $\delta^{34}S_{pyr}$ values show a modest decline from +15‰ to +10‰. $\delta^{34}S_{CAS}$ values from the upper Row Park and lower New Market show a slow steady rise to +29‰, while paired $\delta^{34}S_{pyr}$ values initially rise to as high as +19‰, but dramatically drop to ~+4‰ near the Row Park/New Market boundary. The $\delta^{34}S_{CAS}$ values show a steady drop in the upper New Market and lowermost Chambersburg Formations to +16‰, and then remain relatively invariant (+18 to+20‰) throughout the rest of the Chambersburg. The $\delta^{34}S_{pyr}$ values through this interval initially increase to +14‰ but then become highly variable throughout the Chambersburg Formation (ranging from +2 to +17‰).

The corresponding $\delta^{13}C_{carb}$ values from the Rockdale Run and lower Pinesburg Station Dolomite fluctuate between −2.0 and −4.0‰ and $\delta^{13}C_{org}$ values are invariant near −30.5‰ in these formations. Within the same interval as the first large drop in $\delta^{34}S_{CAS}$ (described above) $\delta^{13}C_{carb}$ values show a steady increase to ~+1.0‰ displaying the rising limb of the Middle Darriwilian carbon isotope excursion (MDICE; Leslie et al., 2011), and $\delta^{13}C_{org}$ shows a corresponding rise to ~−28.3‰ (see also Edwards and Saltzman, 2016). The $\delta^{13}C_{carb}$ and $\delta^{13}C_{org}$ values through the upper Row Park and lower New Market strata decline to −3.0‰ and −30.1‰, respectively. The $\delta^{13}C_{carb}$ values through the overlying New Market and Chambersburg Formations show a slow steady increase to +1.0‰, with $\delta^{13}C_{org}$ values initially increasing to −26.7‰ in the lower New Market Formation, but then upper New Market through Chambersburg Formations values decline to −28.7 to −29.3‰.

4.2. Arbuckle Mountains, Oklahoma

Outcrop exposures along I-35 were sampled continuously, with the uppermost Joins and Oil Creek Formations sampled from previously

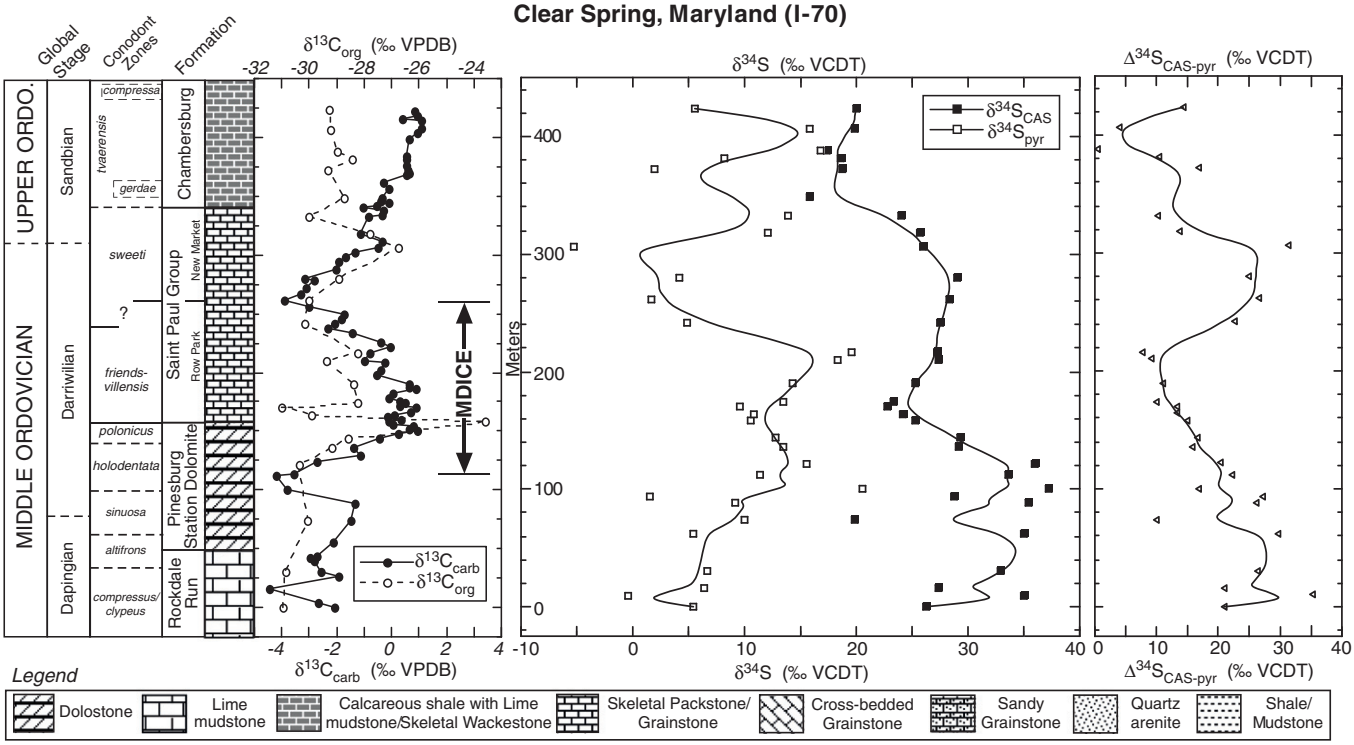

Fig. 2. Middle–Late Ordovician stable isotopic data ($\delta^{34}S_{CAS}$ and $\delta^{34}S_{pyr}$ paired with $\delta^{13}C_{carb}$ and $\delta^{13}C_{org}$) from a road cut along Interstate-70 near the town of Clear Spring, Maryland. Three-point smoothed averages are also plotted for both sulfur isotopic panels. Conodont biozones plotted are from previous biostratigraphic studies (Boger, 1976; Brezinski et al., 1999; Leslie et al., 2013).

well-described exposures in the southern flank of the Arbuckle Anticline (north of Ardmore, OK) and the overlying McLish, Tulip Creek, and Bromide Formations sampled from the northern flank of the Arbuckle Anticline (Bauer, 1990; 2010). The few samples taken from the lower and middle Oil Creek Formation for $\delta^{34}S_{CAS}$ analysis are fairly consistent with values near +30‰ (Fig. 3). The corresponding $\delta^{13}C_{carb}$ and $\delta^{13}C_{org}$ values in the lower Oil Creek initially show significant variability between −2.0 to −4.0‰ and −31.5 to −29.0‰, but in the Middle Oil Creek Formation $\delta^{13}C_{carb}$ and $\delta^{13}C_{org}$ values become less variant, near −2.0‰ and −30.0‰, respectively (Edwards and Saltzman, 2016). The upper Oil Creek Formation was not sampled due to poor exposure, along with the basal quartz arenite of the McLish Formation since it is not suitable lithofacies for $\delta^{34}S$ and $\delta^{13}C$ analyses. Sandy carbonates of the lower McLish (Facies 2A; Bauer, 1990) record $\delta^{34}S_{CAS}$ values of +20‰, with values increasing to +29‰ in the upper McLish (i.e., Facies 6A), although values show variability (3 to 7‰ fluctuations). Paired $\delta^{34}S_{pyr}$ values are also variable through this interval showing no distinctive trend, values from −5 to −19‰ (average ~−12‰). Corresponding $\delta^{13}C_{carb}$ and $\delta^{13}C_{org}$ values increase from −3.0 to +0.75‰ and −30.0 to −27.5‰, respectively. The upper McLish and lower Tulip Creek formations record $\delta^{34}S_{CAS}$ values declining from +29 to +18‰, while $\delta^{34}S_{pyr}$ values increase from −7 to +12‰. The $\delta^{13}C_{carb}$ values are slightly variable (1‰ fluctuations), but decline through this interval from +0.63 to −3.0‰, with few measurements of $\delta^{13}C_{org}$ yielding values from −28.3 to −25.4‰. The overlying Bromide Formation records $\delta^{34}S_{CAS}$ values that range from +24 to +35‰, with $\delta^{34}S_{pyr}$ values initially being light, −5 to −12‰ but then increasing to +5 to +16‰. Corresponding $\delta^{13}C_{carb}$ values show a relatively steady rise from −1.94 to +0.30‰ from the lower to upper Bromide Formation, with $\delta^{13}C_{org}$ values ranging from −30.9 to −28.5‰.

5. Discussion

The large negative shift in $\delta^{34}S_{CAS}$ from mid-Darriwilian strata at Clear Spring and Arbuckle Mountains sections are of similar magnitude (~12‰) to the drop observed in Western Newfoundland (Fig. 4; Thompson and Kah, 2012). This large drop in $\delta^{34}S_{CAS}$ values is coincident with the rising limb and peak $\delta^{13}C_{carb}$ values of the MDICE (Schmitz et al., 2010; Leslie et al., 2011; Albanesi et al., 2013). Another younger large negative drop in $\delta^{34}S_{CAS}$ values (~12‰ magnitude) is recorded in Late Darriwilian–Earliest Sandbian strata in both of our study sections and corresponds to positively trending $\delta^{13}C_{carb}$ values. Although absolute values differ slightly from these sections (Appendix Tables 1 and 2), which may reflect some spatial heterogeneity in the sulfate reservoir, the large-scale trends are consistent with a global change in $\delta^{34}S_{CAS}$ values through the Darriwilian. Previous biostratigraphic investigations place the older negative shift broadly within the *H. holodentata* through *P. polonicus* Conodont Zones and younger drop broadly within *C. sweeti* through lower *A. tvaerensis* Conodont Zones (Boger, 1976; Stouge, 1984; Bauer, 1990, 2010; Brezinski et al., 1999; Albanesi et al., 2013; Leslie et al., 2013). Furthermore, recent SIS investigations of our study sections which were calibrated to the *Geologic Time Scale 2012* (Cooper and Sadler, 2012) constrain the duration of each of these negative shifts in $\delta^{34}S_{CAS}$ to ~3 m.y. (Saltzman et al., 2014; Edwards et al., 2015).

Here we first evaluate factors that may affect the preservation of primary stable isotope signals (i.e., diagenetic alteration, contamination). Having established that our records predominately reflect primary marine chemistry, we go on to interpret the broad-scale trends in $\delta^{34}S_{CAS}$ and $\delta^{13}C$ values and explore possible changes to the environment that could produce these changes in the global sulfur cycle. Geochemical box model simulations are then used to place constraints

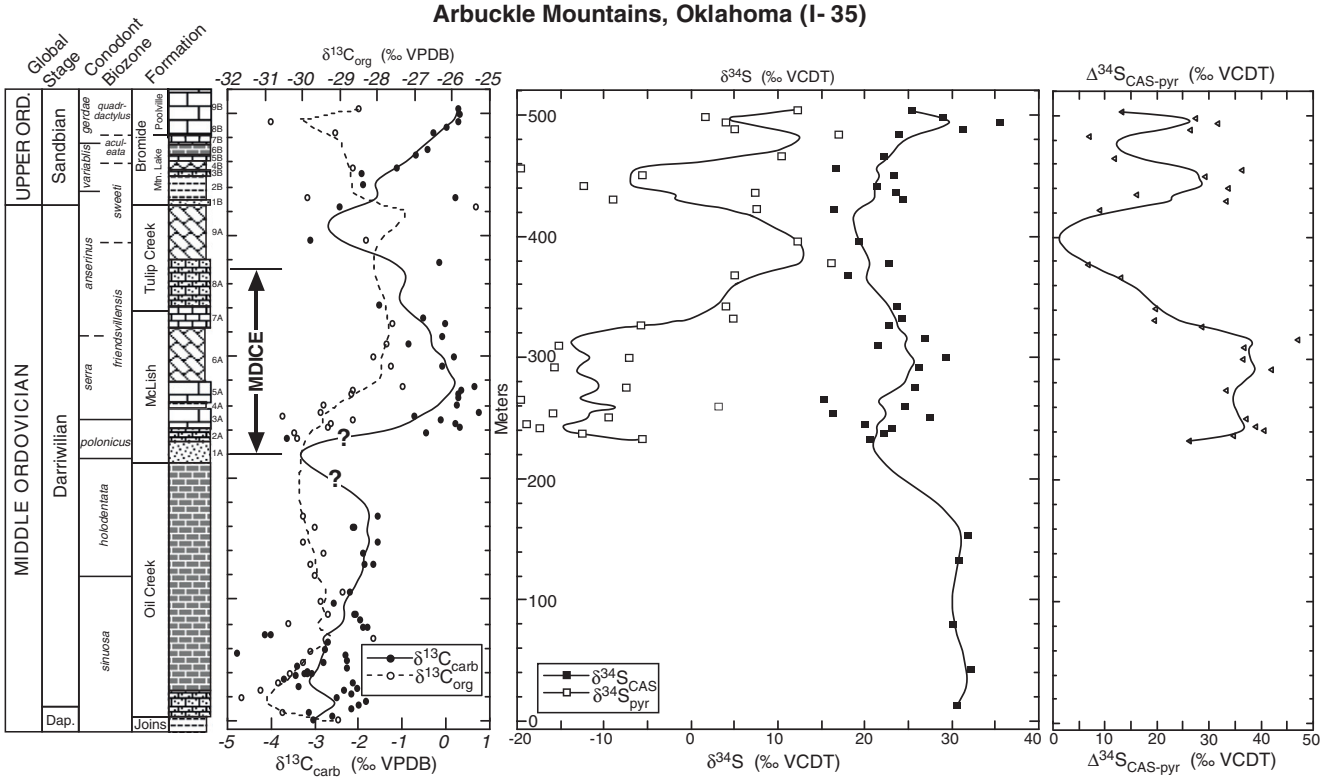

Fig. 3. Middle–Late Ordovician stable isotopic data ($\delta^{34}S_{CAS}$ and $\delta^{34}S_{pyr}$ paired with $\delta^{13}C_{carb}$ and $\delta^{13}C_{org}$) from roadcuts along Interstate-35 within the Arbuckle Mountain region of Oklahoma. Three-point smoothed averages are also plotted for all sulfur and carbon isotopic panels. Conodont biozones plotted are from previous detailed biostratigraphic studies (Bauer, 1987, 1990, 2010). Please note that the exact stratigraphic position of onset of the MDICE is not precisely known due to an unsampled interval in the upper Oil Creek Formation and a thick sandstone unit present in the lower McLish Formation. Also shown on this diagram are the sedimentary lithofacies (1A–9B) defined by Bauer (1990).

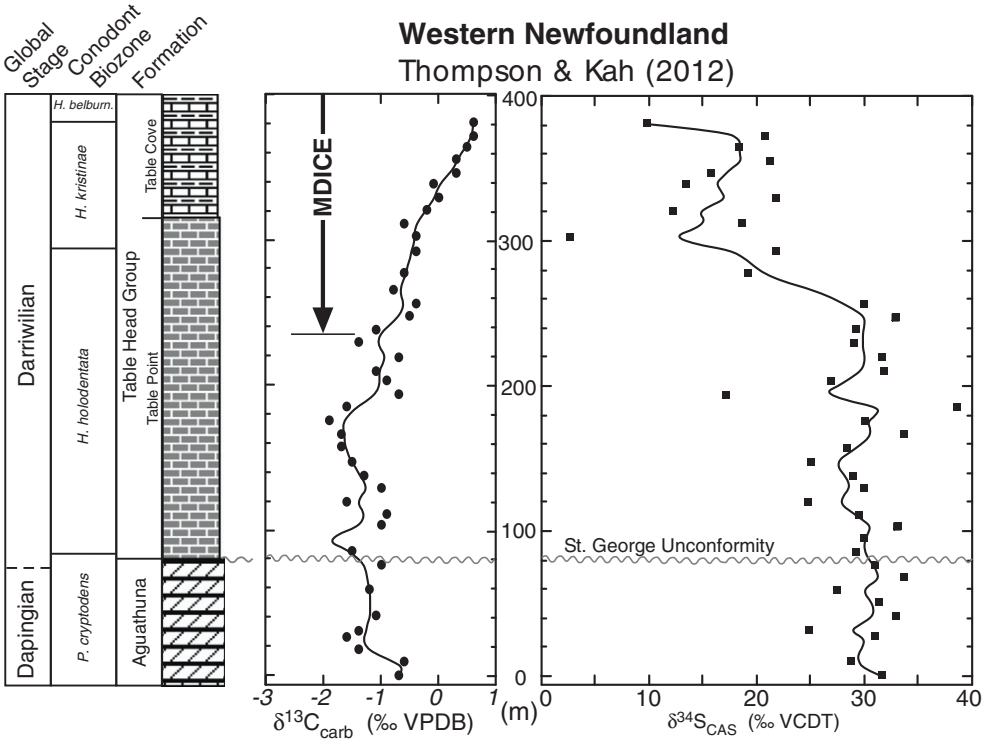

Fig. 4. Replotted Middle Ordovician stable isotopic data ($\delta^{34}S_{CAS}$ and $\delta^{13}C_{carb}$) from previously studied outcrops in Western Newfoundland (Thompson and Kah, 2012). Conodont biozones plotted are from previous biostratigraphic studies (Stouge, 1984; Albanesi et al., 2013).

(e.g., pyrite burial/weathering rates, chemocline migration, sulfate reservoir size) on observed sulfur dynamics during the Darriwilian–Early Sandbian.

5.1. Primary nature geochemical signals

Carbonate rocks undergo burial processes that can potentially affect their geochemical and textural properties. Therefore it is critical to assess ewhether the $\delta^{34}S$ and $\delta^{13}C$ trends are representative of primary seawater signatures. Linear relationships, from cross-plots of seawater proxy geochemical data, are often used to indicate the degree to which carbonate rocks have experienced diagenetic alteration (Given and Lohmann, 1986; Banner and Hanson, 1990; Kaufman et al., 1991). Clear covariation between $\delta^{13}C_{carb}$ and $\delta^{18}O_{carb}$ often indicates influence by meteoric waters, however a cross-plot of our $\delta^{13}C_{carb}$ and $\delta^{18}O_{carb}$ data (Fig. 5B) indicates no significant correlation ($R^2 < 0.1$). Diagenetic alteration of primary $\delta^{13}C_{org}$ values may also occur due to thermal alteration or oxidative loss of certain organic compounds. We observe no systematic relationship ($R^2 < 0.1$) between $\delta^{13}C_{org}$ and wt.% TOC (see Fig. 5A) that might be expected if differential alteration of organic carbon occurred in horizons that are lean versus relatively rich in organic matter. Thus, the lack of significant correlation between our geochemical data and diagenetic proxies suggests preservation of primary marine $\delta^{13}C$ signatures. While much is known about the diagenetic effects on $\delta^{13}C$ and $\delta^{18}O$ values in marine carbonates, fewer investigations have focused on meteoric influences on $\delta^{34}S$. The recent studies of Pleistocene limestones in Florida (Gill et al., 2008) and Late Devonian carbonates of Nevada (Sim et al., 2015) show that meteoric diagenesis significantly lowers CAS concentrations but have little to no effect on $\delta^{34}S_{CAS}$ values recorded within the strata. The absence of correlation between $\delta^{18}O_{carb}$ and [CAS] or $\delta^{18}O_{carb}$ and $\delta^{34}S_{CAS}$ of our studied sections (Fig. 5C and D) suggests that primary marine $\delta^{34}S_{CAS}$ values have not been significantly reset during diagenesis.

It is also important to address concerns regarding incorporation of contaminant sulfate into the CAS fraction. Oxidation of sedimentary pyrite during later stages of diagenesis or chemical extraction of CAS can lower $\delta^{34}S_{CAS}$ values artificially, and linear correlations between $\delta^{34}S_{CAS}$ values and both [S_{pyr}] and $\delta^{34}S_{pyr}$ values could indicate a mixed signature of this contaminant sulfate and primary CAS (Marenco et al., 2008a). However, in cross-plots of our studied sections neither [S_{pyr}] or $\delta^{34}S_{pyr}$ are significantly correlated with $\delta^{34}S_{CAS}$ values ($R^2 \leq 0.2$) and there is no linear correlation between [CAS] and [S_{pyr}] ($R^2 < 0.1$, not plotted), all signifying no obvious influence from pyrite oxidation. Secondary atmospheric sulfate contamination was also minimized in the CAS extraction by employing multiple 24 h water rinsing/leaching steps (Wotte et al., 2012; Peng et al., 2014).

One of the strongest lines of evidence for preservation of primary geochemical signals is the consistency of isotopic trends observed at our two study sections relative to previously published data (Thompson and Kah, 2012), all of which can be correlated independently using conodont biostratigraphy and SIS (Fig. 6). Furthermore, the least radiogenic bulk carbonate $^{87}Sr/^{86}Sr$ values from our Oklahoma section are very close to conodont $^{87}Sr/^{86}Sr$ trends, which is consistent with minimal alteration of carbonates from these sections (Edwards et al., 2015).

The Clear Spring, Maryland section is a mixed dolostone–limestone sequence and the effects of dolomitization on CAS are a potential concern (e.g., Marenco et al., 2008b), however there is no covariance between lithology and [CAS] or $\delta^{34}S_{CAS}$ observed (see Appendix Table 1). Previous studies of Mesoproterozoic and Neoproterozoic dolostone sequences have also argued that dolomitization had little to no effect on $\delta^{34}S_{CAS}$ values (Kah et al., 2004; Hurtgen et al., 2006; Shen et al., 2008). Another concern is the primary nature of the pyrite analyzed within our studied section. Although authigenic pyrite horizons associated with hardgrounds have been documented in some portions of our studied section (e.g., Bromide Formation; Carlucci et al., 2014) we specifically did not sample these intervals for $\delta^{34}S$ analyses. Finally, previous petrographic analyses, comparative sedimentological studies, and lithofacies descriptions (e.g., Lewis, 1982; Mitchell, 1985; Mussman and Read, 1986; Carlucci et al., 2014) of our stratigraphic units support minimal alteration of the studied carbonates.

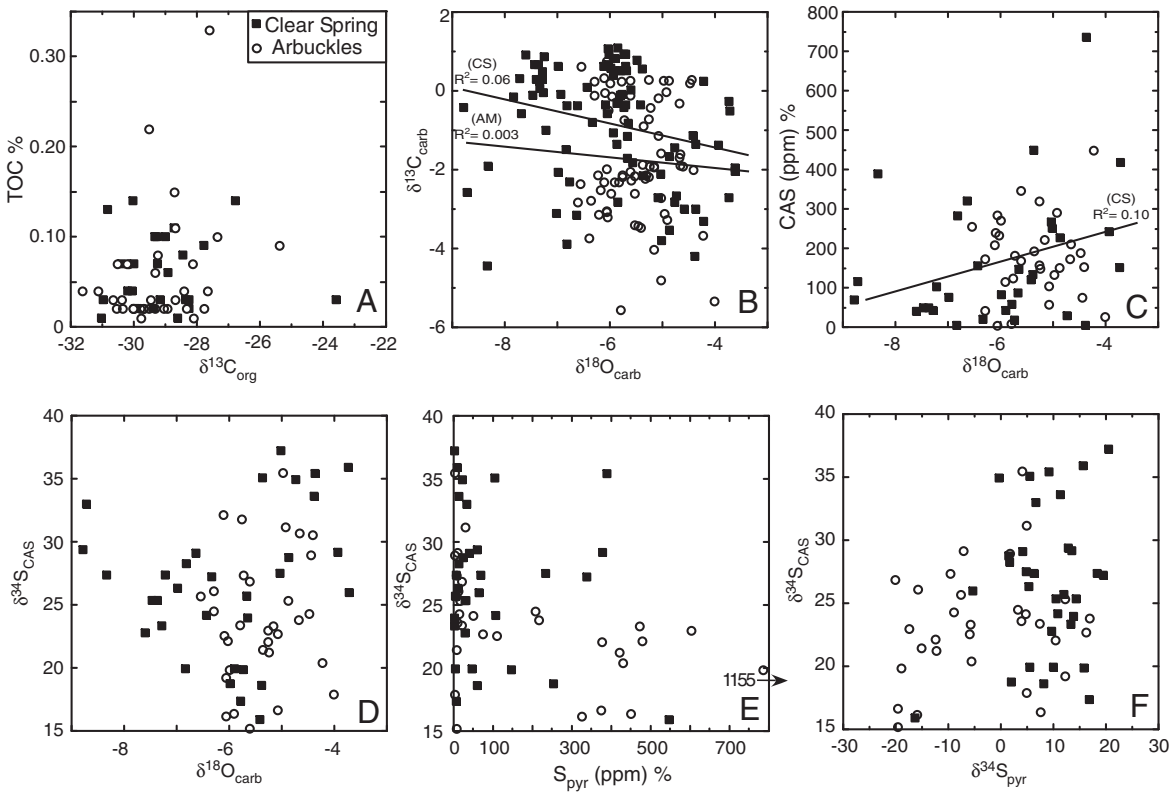

Fig. 5. Cross plots for the evaluation of diagenetic alteration and pyrite oxidation during CAS extractions. A) $\delta^{13}C_{org}$ vs. wt.% TOC, B) $\delta^{13}C_{carb}$ vs. $\delta^{18}O_{carb}$, C) [CAS] vs. $\delta^{18}O_{carb}$, D) $\delta^{34}S_{CAS}$ vs. $\delta^{18}O_{carb}$, E) $\delta^{34}S_{CAS}$ vs. [S_{pyr}], and F) $\delta^{34}S_{CAS}$ and $\delta^{34}S_{pyr}$.

5.2. Possible biogeochemical mechanisms for $\delta^{34}S$ and $\delta^{13}C$ trends

The primary source of sulfur to the global oceans is runoff from oxidative weathering of sulfide minerals and dissolution of sulfate evaporites on the continents (Berner, 1987; Holser et al., 1988). Oxidation of reduced magmatic sulfur (e.g., continental-, arc-, or mid-ocean ridge volcanism) is another import input to the ocean reservoir, although small compared with riverine inputs (Kump, 1989; Alt, 1995; Berner, 2001). Sulfur is primarily removed from the oceans by the deposition of sulfate evaporites and burial of microbially mediated sedimentary pyrite. H_2S produced by MSR is isotopically depleted in ^{34}S by up to 66‰ in laboratory experiments (Harrison and Thode, 1958; Habicht and

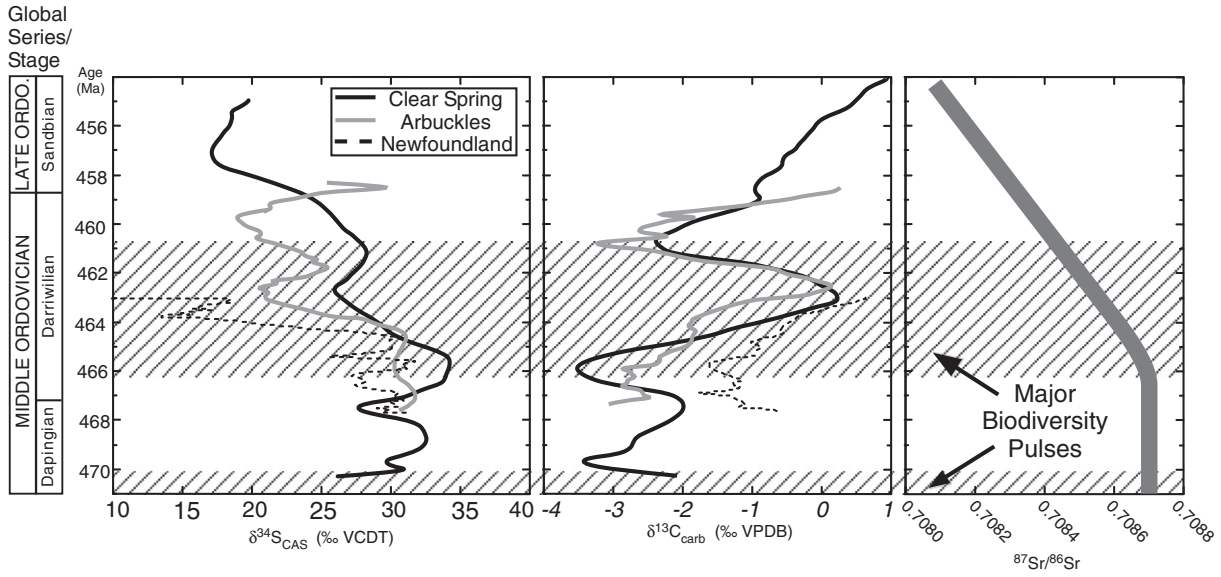

Fig. 6. Three-point smoothed averages of $\delta^{34}S_{CAS}$ and $\delta^{13}C_{carb}$ from our two studied sections, along with the previously investigated Western Newfoundland section (Thompson and Kah, 2012) are scaled to age using age estimates for the bases of conodont zones that have been recently calibrated to the 2012 Geologic Time Scale (Cooper and Sadler, 2012) with seawater $^{87}Sr/^{86}Sr$ stratigraphy (Saltzman et al., 2014). Also plotted is the general seawater $^{87}Sr/^{86}Sr$ trend for the period of the Middle–Late Ordovician. Small apparent offsets in the stable isotopic trends (vertical space) are likely due to imperfect radiometric age constraints on the bases of some conodont zones. Further alignment of these records may be achieved with future higher resolution biostratigraphic and chemostratigraphic studies. Also plotted are approximate levels of the purported two major pulses of biodiversity in the Middle Ordovician (Schmitz et al., 2008; Servais et al., 2008, 2010).

Canfield, 1996; Canfield et al., 2000; Sim et al., 2011a,b), although this fractionation in nature can approach 70‰ in environments such as the Black Sea (Fry et al., 1991). Due to the fact that little to no isotopic fractionation (0–3‰) is associated with sulfur from volcanogenic sources and dissolution–precipitation of evaporites they are not considered to impact isotopic variability of the marine sulfate reservoir significantly (Ault and Kulp, 1959; Thode et al., 1961; Raab and Spiro, 1991). However, burial of sedimentary pyrite, riverine delivery of weathering products of sulfur-bearing minerals, and changes in $\Delta^{34}S$ are considered to be the primary drivers of isotopic change on geologic time scales (Garrels and Lerman, 1984; Berner, 2001; Gomes and Hurtgen, 2013).

Carbon and sulfur cycles are connected through pyrite formation and burial, which is coupled to organic matter burial (Berner and Raiswell, 1983). These processes are linked through microbial sulfate reduction, as the organic matter oxidized during this process is often the limiting reactant in marine environments. The enhanced burial of organic matter can fuel increased MSR and pyrite burial in oxygen-poor waters, although the availability of iron can also play a key role in marine settings (Canfield et al., 1992). In sulfide-rich and oxygen-poor (euxinic) marine environments Fe^{2+} can often be the limiting species in pyrite formation (Lyons et al., 2009). The absence of covariation and presence of antithetical relationships between $\delta^{34}S_{CAS}$ and $\delta^{13}C_{carb}$ trends in our study sections demonstrate that the perturbations of the sulfur cycle could not involve an increase in the pyrite burial flux that might be expected to accompany enhanced organic carbon burial: a potential driver for the MDICE and Early Sandbian rise in $\delta^{13}C_{carb}$ values. Following the reasoning above, the most plausible causal mechanisms for observed Darriwilian–Early Sandbian sulfur and carbon isotope records must involve either increases in the rates of continental runoff, decreases in global burial rates of pyrite, or changes in $\Delta^{34}S$.

5.2.1. Fluctuations in crustal weathering

Tectonic processes and changes in atmospheric O_2 levels that operate on long time scales (>10^6 to 10^7 years) are thought to be the main drivers of crustal weathering fluxes of carbon and sulfur (Garrels and Lerman, 1984; Canfield et al., 2000; Kampschulte et al., 2001). Oxidative weathering of sulfur-bearing minerals, carbonates, and organic-rich sedimentary rocks provide major sources of sulfur and carbon to the oceans. A change in global continental weathering fluxes would affect both carbon and sulfur cycles and would shift both isotope records towards their respective weathering flux values ($\delta^{13}C_{riv} = -4‰$ and $\delta^{34}S_{riv} = +8‰$) (Kump and Garrels, 1986; Kump and Arthur, 1999; Kurtz et al., 2003). A weathering hypothesis has previously been invoked for the latest Ordovician (Hirnantian Stage) positive $\delta^{13}C$ excursion whereby increased weathering of carbonates increased the $\delta^{13}C$ of the weathering flux and subsequently marine $\delta^{13}C_{carb}$ values (Kump et al., 1999). Furthermore, a recent study of Hirnantian carbonates produced paired $\delta^{34}S_{CAS}$ and $\delta^{34}S_{pyr}$ records that were not covariant, with only $\delta^{34}S_{pyr}$ values being in sync with $\delta^{13}C_{carb}$ and $\delta^{13}C_{org}$ trends (Jones and Fike, 2013).

A change in the weathering flux is broadly consistent with sea level lowstands (Sauk–Tippecanoe sequence boundary) recorded throughout the Middle Ordovician (Finney et al., 2007), and a major unconformity (Knox Unconformity) that is widespread in eastern North America displaying >100 m of erosional relief in places (Mussman and Read, 1986). Biostratigraphic evidence also shows maximum sea level lowstand (associated with high continental erosion) occurred within the Mid-Darriwilian globally (Nielsen, 2004; Kanyigan et al., 2010; Dwyer and Repetski, 2012). While the magnitude of sea-level drop in the Darriwilian and Hirnantian are comparable, the magnitude of positive $\delta^{13}C_{carb}$ shifts are not (MDICE +2–3‰ versus HICE +6–7‰) indicating a smaller influence of weathering on marine $\delta^{13}C_{carb}$ values. Varying the $\delta^{34}S$ of the weathering flux was independently rejected by two studies examining mechanisms for Hirnantian $\delta^{34}S_{CAS}$ and $\delta^{34}S_{pyr}$ records (Hammarlund et al., 2012; Jones and Fike, 2013) as they found that the required magnitude of change is unreasonable and also would result in $\delta^{34}S_{CAS}$ and $\delta^{34}S_{pyr}$ trends that parallel one another.

5.2.2. Fluctuations in pyrite burial

Pyrite burial rates are dependent upon water-column redox state, sulfate concentrations, extent of organic matter burial, and Fe^{2+} availability in sedimentary depositional environments (Berner, 1985). The coupled relationship between pyrite and organic matter burial can change if the site of carbon burial shifts out of shallow marine shelf/deltaic environments to settings where pyrite burial rates are lower (Berner and Raiswell, 1983). MSR can be limited in modern ocean settings by the presence of oxygen where product sulfide is oxidized back to sulfate (Canfield, 2001) or lack of reactive organic carbon (Leavitt et al., 2013). Additionally, the availability of Fe^{2+} is often a limiting factor for pyrite formation in shallow water marine sediments (e.g., Canfield et al., 1992). In terrestrial depositional environments (soils, coal swamps, peatlands, some lakes) MSR is limited by the often very low sulfate concentrations (e.g., Goldhaber and Kaplan, 1975; Berner, 1984). Moreover, a study of Early Cenozoic marine carbon and sulfur cycling linked decoupled $\delta^{34}S$ and $\delta^{13}C$ records (isotopically light $\delta^{34}S_{CAS}$ values corresponding to heavy $\delta^{13}C_{carb}$ in Paleocene–Eocene) to enhanced burial of organic carbon in terrestrial environments where sulfate was in short supply and consequently global pyrite burial rates were low (Kurtz et al., 2003). However, a causal mechanism involving terrestrial burial of organic carbon for our inversely related Ordovician stable isotope trends is not likely as these records significantly predate the earliest land plants megafossils and large accumulations of terrestrial organic carbon in the Late Silurian and Devonian, respectively (e.g., Steemans and Wellman, 2004).

Similarly decoupled marine $\delta^{34}S$ and $\delta^{13}C$ records have also been documented from the Early Cretaceous representing periods of decreased pyrite burial and possible shifting of the locus of organic carbon burial (Paytan et al., 2004). Recently basin-wide evaporite deposition has been invoked to explain these inversely related Early Cretaceous $\delta^{34}S$ and $\delta^{13}C$ data, by dramatically lowering oceanic sulfate concentrations and thus reducing pyrite burial rates (Wortmann and Chernyavsky, 2007; Wortmann and Paytan, 2012). Evaporite deposits are found in Ordovician sequences within the Williston Basin (North America), Canning Basin (Australia), and the Siberian Platform (Russia) however they all are of Late Ordovician (Katian Stage) age (Longman et al., 1983; Williams, 1991; Kanyigan et al., 2010a; Husinec and Bergström, 2015). Because these basin-wide evaporites are all significantly younger than our Darriwilian–Early Sandbian $\delta^{34}S$ and $\delta^{13}C$ marine records, large-scale evaporite deposition is unlikely to be linked to a causal mechanism for these perturbations.

As mentioned above, water-column oxygenation may have also significantly limited the burial of pyrite in the Paleozoic (e.g., Leavitt et al., 2013), and the Darriwilian–Early Sandbian $\delta^{34}S_{CAS}$ records presented could plausibly be linked to reduced rates of pyrite formation resulting from fluctuations in the marine redox state. Oxygen levels in the atmosphere–ocean system were thought to have significantly increased in the Late Cambrian as the result of large-scale pyrite and organic carbon burial (Saltzman et al., 2011), although recent studies suggest that Early–Middle Ordovician deep ocean environments were still euxinic and poorly ventilated at times (Thompson and Kah, 2012; Saltzman et al., 2015). Darriwilian–Early Sandbian pyrite burial rates would be mitigated by oceanic ventilation, perhaps driven in part by cooling temperatures (Trotter et al., 2008), that partially oxidized a reactive pool of H_2S in deep ocean settings, resulting in increased delivery of isotopically light sulfate to the global oceans and subsequently a decline in marine $\delta^{34}S_{SO4}$ values. In addition to a decrease of MSR rates, organic matter remineralization rates would have also declined leading to an inverse relationship between burial rates of pyrite and organic carbon, with the marine sulfate reservoir trending towards the $\delta^{34}S$ of the weathering flux (lighter values) while $\delta^{13}C_{carb}$ values increase (e.g., Wortmann and Chernyavsky, 2007).

5.2.3. Fluctuations in $\Delta^{34}S$

There are several factors that influence the isotopic fractionation between sulfate and sedimentary pyrite, and thus stratigraphic trends in $\Delta^{34}S$, they include: sulfate concentration, area of shallow marine environments, reservoir effect in sulfate-limited settings, sulfur disproportionation, cell-specific MSR rates, and restricted exchange of sediment porewater fluids (Habicht and Canfield, 1996, 2001; Habicht et al., 1998, 2002; Canfield, 2001; Lyons et al., 2004; Sim et al., 2011a,b; Gomes and Hurtgen, 2013; Leavitt et al., 2013). Changes in marine sulfate content have been invoked to explain stratigraphic trends in $\Delta^{34}S$ over 10's of m.y. time spans (Fike et al., 2006), as sulfate concentrations in the oceans have drastically changed over the Phanerozoic (e.g., Kah et al., 2004; Gill et al., 2011a; Wortmann and Paytan, 2012). In order to explain these broad $\Delta^{34}S$ trends here sulfate concentrations would have to contract an order of magnitude and return to its previous state two times in the course of ~7–8 m.y. This would necessitate marine sulfate concentrations cycling vacillating between 1–2 mM and 0.1–0.2 mM using the most recent estimates for Early–Middle Ordovician (Thompson and Kah, 2012; see Section 5.3. for further discussion of sulfate concentration).

Additionally, the implications for marine redox state (i.e., low $\Delta^{34}S$ values linked to reduced O_2 levels in marine environments) are inconsistent with large pulses of biodiversity in the Middle Ordovician (Servais et al., 2008, 2010). Sulfur isotope systematics in lacustrine and restricted marine settings show that $\Delta^{34}S$ values in these systems are significantly affected by the amount of sulfate consumed during MSR and the location of pyrite formation (Sælen et al., 1993; Gomes and Hurtgen, 2015). In low-sulfate euxinic systems isotopic distillation (Rayleigh fractionation) of the sulfate reservoir and sulfide product can occur and strongly influence their $\delta^{34}S$ values, thus $\Delta^{34}S$ values could reflect how restricted a local basin may be, as a major requirement for this reservoir effect is closed-system sulfur cycling under stratified water masses (Sælen et al., 1993; Gomes and Hurtgen, 2013). The overall shallowing-upward trends (representing transition to more restricted peritidal to subtidal carbonate environments) in the Rockdale Run through Row Park formations and shallowing of facies from lower to upper McLish Formation support a reservoir effect explanation for the coincident declining $\Delta^{34}S$ values. However, lithofacies/sequence stratigraphic interpretations of latest Darriwilian–Early Sandbian strata from our study sections show a rise in sea-level and return to more open-ocean conditions (Bauer, 1990; Brezinski et al., 2012), yet $\Delta^{34}S$ values in Maryland show a declining trend which is not consistent with a reservoir effect linked to changes in depositional environment. Late Sandbian Bromide (Pooleville Member) strata show overall regressive set of lithofacies and a return to restricted settings, although $\Delta^{34}S$ values remain high, which is also inconsistent with reservoir effect being the predominant factor influencing these trends.

High metabolic rates of MSR produce small sulfur isotope fractionations, while low rates result in large fractionations (≥ net fractionation for sulfur disproportionation) between sulfate and sulfide (Harrison and Thode, 1958; Kaplan and Rittenberg, 1964; Goldhaber and Kaplan, 1975; Sim et al., 2011a,b; Leavitt et al., 2013). Variations in the global average cell-specific MSR rate have been invoked to explain declines in $\Delta^{34}S$ trends in the Late Devonian linked either to increased availability of labile organic matter or change in microbial composition (John et al., 2010). Recent experimental work on MSR has linked $\delta^{34}S$ fractionation rates to availability of organic matter in sedimentary environments and areal extent of shallow marine environments (Leavitt et al., 2013). However, in the Early/Middle Paleozoic Leavitt et al. (2013) found no correlation with available continental shelf to sulfur isotope fractionations ($\Delta^{34}S$ trends) suggesting that other abiotic and biotic processes (previously discussed this section) are likely significantly impacting our Ordovician $\Delta^{34}S$ values.

Chemocline depth within the sediments can also significantly impact $\Delta^{34}S$ trends. If this redox boundary deepens within the sediments then porewaters become relatively isolated from the overlying water column. Therefore, $\delta^{34}S_{pyr}$ and $\delta^{34}S_{CAS}$ records represent distinct pools of sulfur, porewater sulfate (sedimentary pyrite) and marine sulfate (CAS), that evolved independently from one another (Lyons et al., 2004). Subsequently, our $\Delta^{34}S$ trends that track $\delta^{34}S_{CAS}$ values could reflect migration of the chemocline further into the sediments leading to declines in pyrite burial during the transition to more oxic conditions (e.g., Jones and Fike, 2013).

5.3. Controls on sulfur cycling in the Darriwilian–Early Sandbian

To further test the above scenarios for the mechanisms behind the sulfur isotope record, we constructed a forward box model of the Middle–Late Ordovician sulfur cycle. Here the boundary conditions for the sulfur cycle were initially set and later perturbed during the model runs in order to recreate the observed sulfate sulfur isotope profile. Model solutions were deemed valid if they reproduced the sulfate sulfur isotope record both in timing and magnitude. The following expressions for the change in the mass and isotopic composition of sulfate in the ocean over a given time interval were used in the model (see Gill et al. (2011a,b) and Kurtz et al. (2003) for additional details of this formulation):

$$\frac{\partial M_O}{\partial t} = F_W - F_{py} - F_{gyp}$$
$$\frac{\partial \delta_O}{\partial t} = \frac{F_W(\delta_W - \delta_O) - F_{py}\Delta S}{M_O}$$

where M_o and δ_o are the amount of sulfate-S in the ocean reservoir and its isotopic composition, respectively. Estimates for the concentration of marine sulfate (and thus M_o) vary from less than 2 mM in the Early Ordovician (Thompson and Kah, 2012) up to potentially 10 mM in the Late Ordovician (Jones and Fike, 2013). Further estimates for marine sulfate concentrations come from Horita et al. (2002) who estimated a range of 4 to 15 mM later in the Silurian. The input to the ocean, *Fw*, represents the combined fluxes of sulfur delivered to the ocean via weathering of the continents and magmatic processes. These fluxes are combined together in F_W because their isotopic compositions—defined as δw in the model—are similar. F_{gyp} represents the flux of sulfate out of the ocean as sulfate minerals. F_{py}, representing the output of sulfur from the ocean through the burial pyrite and ΔS represents the difference in isotope composition between marine sulfate and that pyrite. The values explored for these various parameters in the model are shown in Table 3.

An additional aspect of our box model that is applied in some of our modeling runs allows the removal of fluxes of sulfate from the ocean to dynamically scale with the size of the marine sulfate reservoir; the sinks (outside of forced perturbations involving these fluxes) are dependent on the mass of the marine sulfate reservoir. This introduces an important negative feedback on the output fluxes which are linked to the size of the sulfate reservoir. In the model, the output fluxes follow a first order rate law (Lasaga, 1980; Lasaga and Berner, 1998):

$$F = kM_O$$

where *F* refers to either of the output fluxes (F_{py} or F_{gyp}) and *k* is a rate constant that is dependent on the initial model boundary conditions. Note that for each initial M_O, new *k* values are calculated for the initial steady state for each model run.

Broadly we can reproduce the two observed declines in the sulfate sulfur isotope record during the Darriwilian–Early Sandbian with transient changes to the sulfur cycle. These transient changes were implemented in the model for duration consistent with estimates of the declines in seawater $\delta^{34}S_{SO4}$ record ($\delta^{34}S_{CAS}$ values); roughly 3 m.y. each with a million year relaxation interval in between them. Drivers we explored in the model include: 1) increasing the weathering flux of sulfate to the ocean (F_w), 2) reducing burial rate of pyrite sulfur (F_{py}), and 3) decreasing the isotopic difference between seawater

sulfate and sedimentary pyrite ($\Delta^{34}S$). We consider and evaluate each of these scenarios below.

The Darriwilian declines in $\delta^{34}S_{SO4}$ record can be reproduced by two transient increases of F_W by 2 to 6 times, lasting 3 m.y. each (see model Figs. 7 and 8 for a sensitivity test that explore increases in F_W). The magnitude of the change of this flux needed to recreate the observed isotope record is directly dependent on the initial model state, particularly the size of the sulfate reservoir. Estimates for the size of the sulfate reservoir vary from less than 2 mM to 10 mM (Thompson and Kah, 2012; Jones and Fike, 2013). It is important to note here that acceptable solutions were only achieved if 1) the isotope composition of the weathering flux (δ_w) was set at the low end of values (0‰ to +5‰) thought to be representative of this flux (Table 3) and 2) the output fluxes (F_{py} or F_{gyp}) do not scale dynamically with the size of the sulfate reservoir (compare Figs. 7 to 8). Model runs with higher δ_w need unreasonable large increases in F_w (6 times the modern weathering flux of sulfur or greater) to produce the observed declines in the $\delta^{34}S$ of marine sulfate.

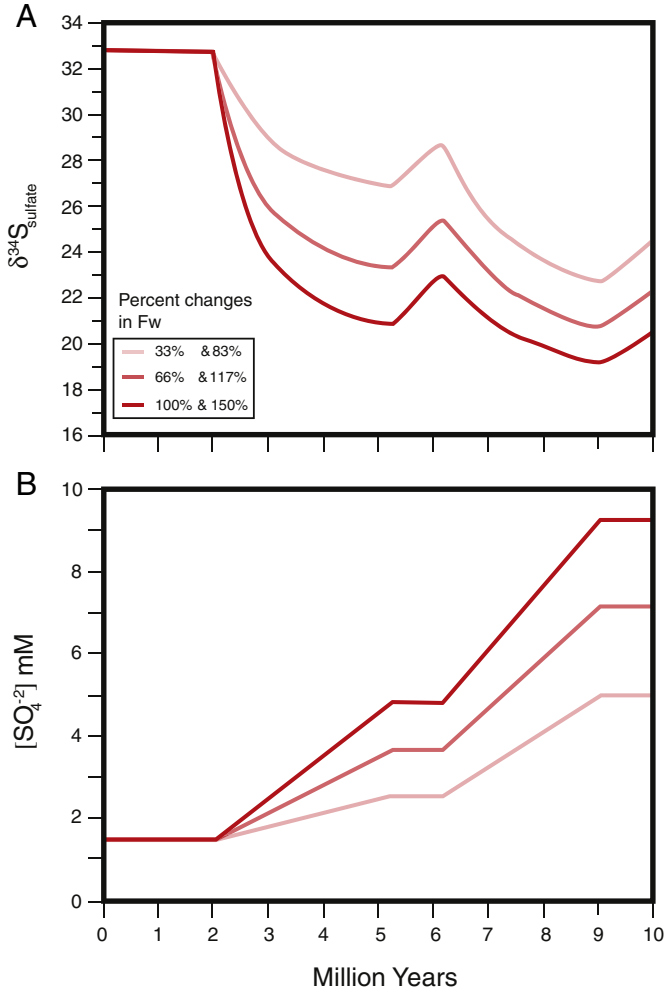

Fig. 7. Simulations showing the effect of varying the magnitude of the transient increase in sulfate weathering flux (F_w) during the Middle Ordovician. A) is modeled seawater $\delta^{34}S$ response to increases in F_w and B) is modeled response to global seawater sulfate reservoir. In these simulations the output fluxes F_{py} and F_{gyp} do not scale with the size of the marine sulfate reservoir. Labels denote the percent increase in F_w from the initial steady-state rates. In these simulations, the initial marine sulfate concentration was 1.5 mM. Note that in these simulations (Figs. 7, 8, 9), either pyrite burial (F_{py}) was decreased or the F_w was increased transiently for 3 m.y. at the 2 and 6.2 million year time points in each model run. Note that the figured simulations are intended to demonstrate the effect of altering some of the parameters within the model and not to display all possible or even valid solutions.

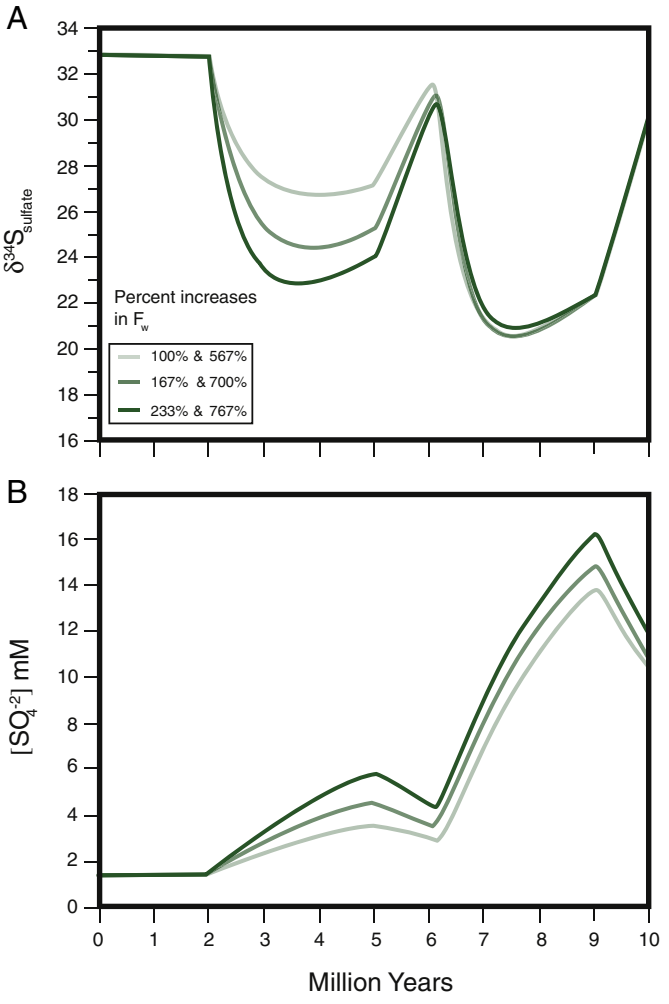

Fig. 8. Simulations showing the effect of varying the magnitude of the transient increase in sulfate weathering flux (F_w) during the Middle Ordovician. A) is modeled seawater $\delta^{34}S$ response to increases in F_w and B) is modeled response to global seawater sulfate reservoir. In these simulations the output fluxes F_{py} and F_{gyp} are allowed a scale with the size of the marine sulfate reservoir. Labels denote the percent increase of F_w from the initial steady-state rates. In these simulations, the initial marine sulfate concentration was 1.5 mM.

It is also noteworthy that changing the δ_w alone could not produce the observed isotope records. Runs where the output fluxes scaled with the size of the sulfate reservoir needed unrealistically large (8 times or greater) F_w increases to reproduce the observed trends. These exercises also produced large sulfate reservoir sizes (compare Figs. 7 to 8) that are inconsistent with other estimates predicted for the Ordovician oceans (Thompson and Kah, 2012; Jones and Fike, 2013). This suggests that increases in F_w may not be a viable driver since other scenarios (decreasing F_{py} and/or decreasing ΔS) with these dynamic fluxes included in the model produce acceptable solutions.

Additionally, any major change in the riverine flux of C and S should be recognizable from continental weathering proxy records (e.g., seawater $^{87}Sr/^{86}Sr$ records). A dramatic decline in Ordovician seawater $^{87}Sr/^{86}Sr$ values begins within the *P. polonicus–P. serra* Zones, suggesting the start of major changes in long-term weathering fluxes in the Middle Darriwilian (Young et al., 2009; Saltzman et al., 2014). Additionally, ε_{Nd} values from graptolitic shales at the base of the Taconic foreland basin sequence indicates a change in source rock weathering in the region beginning in the Late Darriwilian (*Didymograptus murchisoni* graptolite zone; Gleason et al., 2002). Sequence stratigraphic and sedimentologic evidence is most consistent for increased

continental runoff during the Middle Darriwilian (older modeled increase of F_w). The latest Darriwilian–Early Sanbian strata (younger modeled increase of F_w) show evidence of global sea level rise, while continental weathering proxy records of seawater $^{87}Sr/^{86}Sr$ and ε_{Nd} indicate that enhanced erosion of young volcanic and igneous rocks associated with the Taconic orogeny was still ongoing. Therefore, transient increases in F_w may remain a potential causal mechanism for these sulfur cycle perturbations, although they are not necessarily favored as the dominant influence on $\delta^{34}S$ at this time due to complicated linkages to sea level histories, weathering proxies, rationale for lowered δ_w values and the failure of our model with dynamic output fluxes to reproduce the $\delta^{34}S$ record.

Alternatively, we can reproduce the declines in the $\delta^{34}S_{SO4}$ record by two transient decreases of F_{py} lasting 3 m.y. each (see Fig. 9 for a sensitivity test that explores decreases in F_{py}). The magnitude of these reductions needs to be 20% to 80% times the pre-MDICE F_{py} flux, depending on the initial model conditions (size of M_o, value for ΔS). It should be mentioned that needed decreases in F_{py} can be lessened if we also simultaneous decrease the ΔS term with the decreases of the F_{py} term (see more discussion of this below). Further support for the reduced pyrite burial linked to ocean ventilation can be found when looking at our $\delta^{34}S_{pyr}$ records that seem to broadly track $\delta^{13}C_{carb}$ values and not $\delta^{34}S_{CAS}$ data. These pulses of oceanic ventilation would have pushed the chemocline deeper within the sediments, resulting in restricted porewater communication with the overlying water column leading to the gradual enrichment $\delta^{34}S_{pyr}$ as sedimentary pyrite continued to form. Interestingly, Hirnantian $\delta^{34}S_{pyr}$ records from China were recently interpreted to reflect similar water-column oxygenation phenomenon (Yan et al., 2009).

Lastly we found that a transient lowering of $\Delta^{34}S$ alone also could produce the Darriwilian declines in the $\delta^{34}S$ sulfate record. Sensitivity testing of the model shows that transient decreases in ΔS to values of 25‰ or less lasting 3 m.y. each could produce acceptable modeling solutions (Fig. 10). Changing rates of MSR have been recently invoked to explain a drop in $\Delta^{34}S$ trends through the Hirnantian (latest Ordovician) coincident with glacial maximum, whereby cooler temperatures promoted decreased aerobic decomposition of organic matter that led to increased MSR rates (Jones and Fike, 2013). However, there are no known glacial deposits of Darriwilian–Sandbian age (e.g., Frakes et al., 1992) and sea surface temperatures were thought to be relatively consistent (Trotter et al., 2008) suggesting climate induced cell-specific MSR rate changes are an unlikely explanation for declining $\Delta^{34}S$ values. Deepening of the zone of sulfate reduction within the sediments could explain this modeling scenario, with our $\Delta^{34}S$ record resulting from increasing closed system isotope behavior of the sulfur in sedimentary pore waters during the transition to more oxic conditions.

Although we have presented scenarios where a single driver is responsible for generating the observed isotope record, it is important to point out that two or more of these potential drivers can also be changed simultaneously to produce the observed isotope record. For example, a scenario where both F_{py} and $\Delta^{34}S$ are simultaneously decreased is attractive since ocean ventilation would conceivably decrease both the rates of pyrite burial and $\Delta^{34}S$ for reasons articulated above. With this in mind, and given our results from our single driver modeling exercises, we advocate ocean ventilation as the primary driver of the Darriwilian–Early Sandbian $\delta^{34}S$ sulfate record. Additionally, although

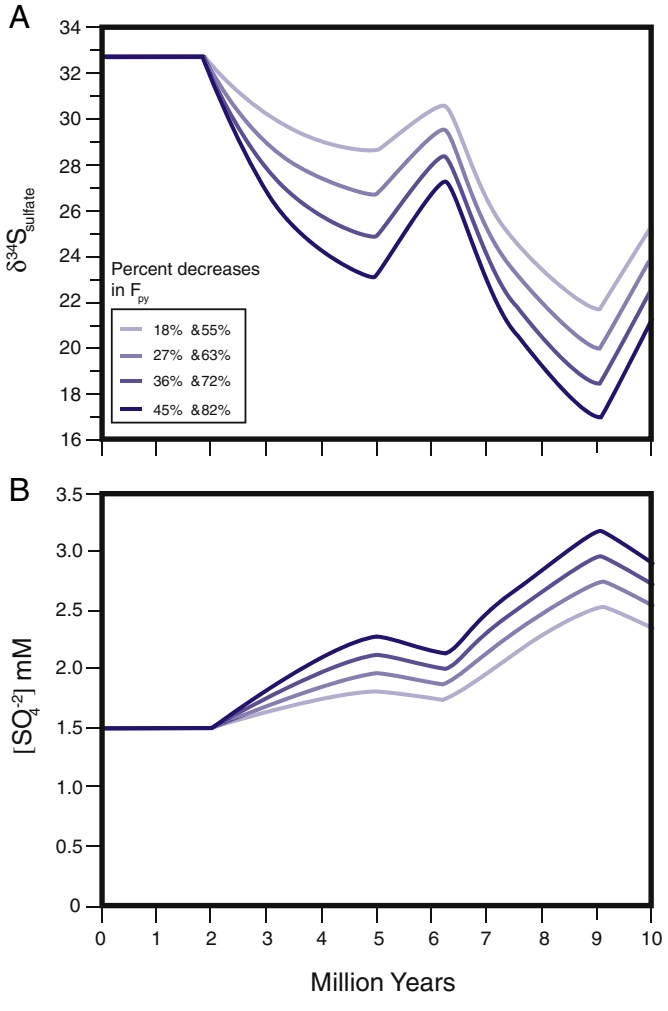

Fig. 9. Simulations showing the effect of varying the magnitude of the transient decrease in pyrite burial (F_{py}) during the Middle Ordovician. A) is modeled seawater $\delta^{34}S$ response to increases in F_w and B) is modeled response to global seawater sulfate reservoir. In these simulations the output fluxes F_{py} and F_{gyp} are allowed a scale with the size of the marine sulfate reservoir outside the intervals of the forced decreases in F_{py}. Labels denote the percent decrease in F_{py} from the initial steady-state rates. In these simulations, the initial marine sulfate concentration was 1.5 mM. Note the difference in scale of the sulfate concentration from Figs. 7B and 9B.

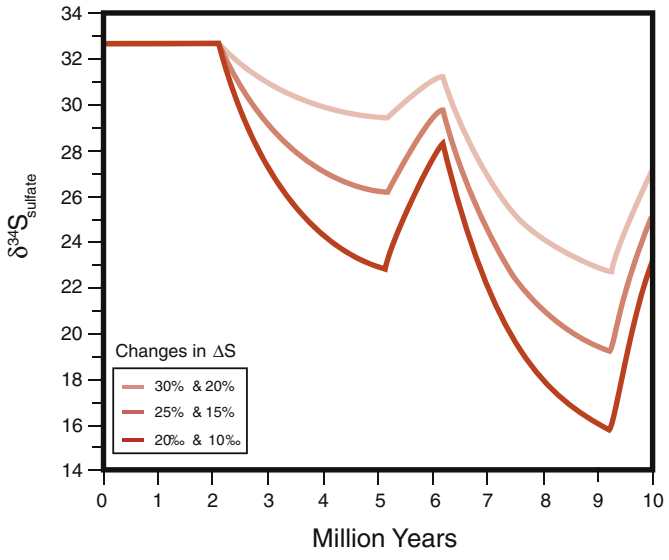

Fig. 10. Simulations showing the effect of transiently changing $\Delta^{34}S$ during the Middle Ordovician. Figure displays the modeled seawater $\delta^{34}S$ response to decreases in $\Delta^{34}S$. In these simulations, since there was no change in the mass balance, there was no change in the size of the marine sulfate reservoir; marine sulfate concentration used here was 1.5 mM. Labels denote the new transiently applied value for $\Delta^{34}S$ during each perturbation.

we recognize that changes in F_w may have contributed to some degree to the observed sulfur isotopic trends, we consider relatively short-term pulses of ocean oxygenation to be the most plausible scenario for generating two distinct $\delta^{34}S_{CAS}$ excursions separated by ~1 m.y.

Another key aspect of our modeling results are that they give estimates of the size of the Darriwilian–Sandbian marine sulfate reservoir. Broadly, the magnitude of changes to the sulfur cycle needed to recreate the observed $\delta^{34}S_{CAS}$ record are directly dependent on the initial size of the marine sulfate reservoir (i.e., the larger the reservoir the larger the necessary changes in F_{py}, ΔS and F_w). Sensitivity testing of our model suggests that marine sulfur reservoir at the start of the Darriwilian was likely 5 mM or less. These concentrations are in line with estimates for marine sulfate during the Early to Middle Ordovician (Thompson and Kah, 2012).

From of our modeling results we can also draw conclusions about possible changes in the size of the marine sulfate reservoir. If we invoke either decreasing F_{py} or increasing F_w in the Darriwilian–Early Sandbian $\delta^{34}S_{SO4}$ record, these changes in the sulfur cycle result in a growth of the marine sulfate reservoir (Figs. 7 and 9). This result is broadly consistent with the recent estimates for marine sulfate concentration over the Ordovician (Thompson and Kah, 2012; Jones and Fike, 2013). Based on their $\delta^{34}S$ records, Thompson and Kah (2012) argue for low marine sulfate concentrations (<2 mM) during the early portion of the Ordovician (Tremadocian to Darriwilian) and by the Late Ordovician, marine sulfate concentrations are suggested to have been at least 5 mM (Jones and Fike, 2013). Across our acceptable modeling solutions the marine sulfate reservoir grows by 2 to 5 mM. Thus our modeling exercises lend support to the notion of a small but notable growth of the marine sulfate reservoir during this period of the Ordovician.

6. Implications and conclusions

Our Middle–Late Ordovician paired $\delta^{34}S$ and $\delta^{13}C$ data and geochemical modeling study improve our understanding of the coevolution of the global sulfur and carbon cycles. The antithetically related Darriwilian–Early Sandbian stable isotope records are similar to other decoupled $\delta^{34}S$ and $\delta^{13}C$ trends observed later during the Phanerozoic (Wortmann and Chernyavsky, 2007; Wortmann and Paytan, 2012) and were likely the product of a reduction of the burial rates of pyrite and organic matter remineralization and fairly low seawater sulfate concentrations (≤10 mM; Horita et al., 2002; Lowenstein et al., 2005; Gill et al., 2007). Furthermore, these Darriwilian–Early Sandbian records represent a critical transition between low marine sulfate concentrations in the Early Ordovician and increased concentrations in the latest Ordovician (Thompson and Kah, 2012; Jones and Fike, 2013). These successive drops in $\delta^{34}S_{CAS}$ may have been caused by decreases in the burial rate of pyrite driven by water-column oxygenation associated with long-term trends in organic carbon burial and global temperatures. Ocean ventilation can fundamentally link our trends in $\Delta^{34}S$ values to a reduction of F_{py} to explain our large declines in seawater $\delta^{34}S_{SO4}$ records. This mechanism is consistent with a progressive cooling of Ordovician oceans (Trotter et al., 2008) that could incorporate more dissolved oxygen. Pulses of ocean ventilation provide a plausible mechanism to explain the $\delta^{34}S$ and $\delta^{13}C$ records, and have broad-scale implications for the marine biosphere. Increased ventilation of marine environments would have provided more habitable settings for organisms to expand into, and is largely consistent with large surges of biodiversity in the Middle Ordovician (e.g., Servais et al., 2008, 2010). The capacity of the marine biosphere to mediate pyrite formation and remineralize organic matter was significantly affected by these environmental changes. The declines in pyrite and organic carbon burial, although not concurrent (inversely related $\delta^{34}S$ and $\delta^{13}C$ records), would also reduce the fluxes of O_2 to the ocean–atmosphere system, consistent with the view that redox conditions in parts of the oceans cycled from oxic to anoxic/euxinic as part of a long-term Early Paleozoic transition.

Acknowledgments

We thank Benjamin Underwood, Jade Marks, and Peter Sauer for technical assistance with isotope analyses at SIRF-Indiana University at Bloomington. Additionally, we thank Jeff Bauer, Stig Bergström, and John Repetski for access to samples and help with fieldwork. SAY gratefully acknowledges the research support from Indiana University and insightful discussions with Lisa Pratt. We thank Guest Editor Thomas Algeo and two anonymous reviewers for their very thoughtful comments that helped strengthen the manuscript.

Appendix A. Supplementary data

Supplementary data to this article can be found online at http://dx.doi.org/10.1016/j.palaeo.2015.09.040.

References

Achab, A., Paris, F., 2007. The Ordovician chitinozoan biodiversification and its leading factors. Palaeogeogr. Palaeoclimatol. Palaeoecol. 245 (1–2), 5–19.
Albanesi, G.L., Bergstrom, S.M., Schmitz, B., Serra, F., Feltes, N.A., Voldman, G.G., Ortega, G., 2013. Darriwilian (Middle Ordovician) delta C-13(carb) chemostratigraphy in the Precordillera of Argentina, Documentation of the Middle Darriwilian Isotope Carbon Excursion (MDICE) and its use for intercontinental correlation. Palaeogeogr. Palaeoclimatol. Palaeoecol. 389, 48–63.
Alt, J.C., 1995. Sulfur isotopic profile through the oceanic-crust — sulfur mobility and seawater–crustal sulfur exchange during hydrothermal alteration. Geology 23 (7), 585–588.
Ault, W.U., Kulp, J.L., 1959. Isotopic geochemistry of sulphur. Geochim. Cosmochim. Acta 16 (4), 201–235.
Banner, J.L., Hanson, G.N., 1990. Calculation of simultaneous isotopic and trace-element variations during water–rock interaction with applications to carbonate diagenesis. Geochim. Cosmochim. Acta 54 (11), 3123–3137.
Barnes, C.R., 2004. Was there an Ordovician superplume event? In: Webby, B.D., Paris, F., Droser, M.L., Percival, I.G. (Eds.), The Great Ordovician biodiversification event. Columbia University Press, New York, pp. 77–80
Bauer, J.A., 1987. Conodonts and conodont biostratigraphy of the McLish and Tulip Creek Formations (Middle Ordovician) of South-Central Oklahoma. Okla. Geol. Surv. Bull. 141, 58.
Bauer, J.A., 1990. Stratigraphy and conodont biostratigraphy of the Upper Simpson Group, Arbuckle Mountains, Oklahoma. Oklahoma Geological Survey Guidebook vol. 27 pp. 39–53.
Bauer, J.A., 2010. Conodonts and conodont biostratigraphy of the Joins and Oil Creek Formations, Arbuckle Mountains, south-central Oklahoma. Okla. Geol. Surv. Bull. 150, 1–44.
Berner, R.A., 1984. Sedimentary pyrite formation: An update*. Geochimica Et Cosmochimica Acta 48, 605–615.
Berner, R.A., 1985. Sulfate reduction organic-matter decomposition and pyrite formation. Philos. Trans. R. Soc. A Math. Phys. Eng. Sci. 315 (1531), 25–38.
Berner, R.A., 1987. Models for carbon and sulfur cycles and atmospheric oxygen — application to Paleozoic geologic history. Am. J. Sci. 287 (3), 177–196.
Berner, R.A., 2001. Modeling atmospheric O-2 over Phanerozoic time. Geochim. Cosmochim. Acta 65 (5), 685–694.
Berner, R.A., 2004. The Phanerozoic carbon cycle: CO_2 and O_2. Oxford University Press, New York.
Berner, R.A., Raiswell, R., 1983. Burial of organic–carbon and pyrite sulfur in sediments over Phanerozoic time — a new theory. Geochim. Cosmochim. Acta 47 (5), 855–862.
Boger, J.B., 1976. Conodont Biosratigraphy of the Upper Beekmantown Group and the St. Paul Group (Middle Ordovician) of Maryland and West Virginia (M.S. Thesis), The Ohio State University (360 pp.).
Brezinski, D.K., 1996. Carbonate ramps and reefs: Paleozoic stratigraphy and paleontology of western Maryland. Maryland Geological Survey Geologic Guidebook 6 p. 25.
Brezinski, D.K., Repetski, J.E., Taylor, J.F., 1999. Stratigraphic and paleontologic record of the Sauk III regression in the central Appalachians. In: Santucci, V.L., McClelland, L. (Eds.), National Park Service Paleontological Research Technical Report 4, pp. 32–41.
Brezinski, D.K., Repetski, J.E., Taylor, J.F., 2012. Sequential development of platform to off-platform facies of the Great American carbonate bank in the Central Appalachians. In: Derby, J.R., Fritz, R.D., Longacre, S.A., Morgan, W.A., Sternbach, C.A. (Eds.), The Great American Carbonate Bank: The Geology and Economic Resources of the Cambrian–Ordovician Sauk Megasequence of Laurentia. Association of American Petroleum Geologists Memoir 98, pp. 383–420.
Bruchert, V., Pratt, L.M., 1996. Contemporaneous early diagenetic formation of organic and inorganic sulfur in estuarine sediments from St Andrew Bay, Florida, USA. Geochim. Cosmochim. Acta 60 (13), 2325–2332.
Buggisch, W., Keller, M., Lehnert, O., 2003. Carbon isotope record of Late Cambrian to Early Ordovician carbonates of the Argentine Precordillera. Palaeogeogr. Palaeoclimatol. Palaeoecol. 195 (3–4), 357–373.
Burdett, J.W., Arthur, M.A., Richardson, M., 1989. A neogene seawater sulfur isotope age curve from calcareous pelagic microfossils. Earth Planet. Sci. Lett. 94 (3–4), 189–198.
Canfield, D.E., 2001. Biogeochemistry of sulfur isotopes. Stable Isot. Geochem. 43, 607–636.

Canfield, D.E., Raiswell, R., Westrich, J.T., Reaves, C.M., Berner, R.A., 1986. The use of chromium reduction in the analysis of reduced inorganic sulfur in sediments and shales. Chem. Geol. 54 (1–2), 149–155.
Canfield, D.E., Raiswell, R., Bottrell, S., 1992. The reactivity of sedimentary iron minerals toward sulfide. Am. J. Sci. 292 (9), 659–683.
Canfield, D.E., Habicht, K.S., Thamdrup, B., 2000. The Archean sulfur cycle and the early history of atmospheric oxygen. Science 288 (5466), 658–661.
Canfield, D.E., Poulton, S.W., Narbonne, G.M., 2007. Late-Neoproterozoic deep-ocean oxygenation and the rise of animal life. Science 315 (5808), 92–95.
Canfield, D.E., Poulton, S.W., Knoll, A.H., Narbonne, G.M., Ross, G., Goldberg, T., Strauss, H., 2008. Ferruginous conditions dominated later neoproterozoic deep-water chemistry. Science 321 (5891), 949–952.
Cardenas, A.L., Harries, P.J., 2010. Effect of nutrient availability on marine origination rates throughout the Phanerozoic eon. Nat. Geosci. 3 (6), 430–434.
Carlucci, J.R., Westrop, S.R., Brett, C.E., Burkhalter, R., 2014. Facies architecture and sequence stratigraphy of the Ordovician Bromide Formation (Oklahoma): a new perspective on a mixed carbonate-siliciclastic ramp. Facies 60 (4), 987–1012.
Cooper, R.A., Sadler, P.M., 2012. The Ordovician Period. In: Gradstein, F.M., Ogg, J.G., Schimtz, M.D., Ogg, G.M. (Eds.), The Geologic Time Scale 2012. Elsevier, Amsterdam, pp. 489–523.
Denison, R.E., Koepnick, R.B., Burke, W.H., Hetherington, E.A., 1998. Construction of the Cambrian and Ordovician seawater Sr-87/Sr-86 curve. Chem. Geol. 152 (3–4), 325–340.
Droser, M.L., Finnegan, S., 2003. The Ordovician radiation: a follow-up to the Cambrian explosion? Integr. Comp. Biol. 43 (1), 178–184.
Droser, M.L., Bottjer, D.J., Sheehan, P.M., 1997. Evaluating the ecological architecture of major events in the Phanerozoic history of marine invertebrate life. Geology 25 (2), 167–170.
Dwyer, G.S., Repetski, J.E., 2012. The Middle Ordovician Knox Unconformity in the Black Warrior Basin. In: Derby, J.R., Fritz, R.D., Longacre, S.A., Morgan, W.A., Sternbach, C.A. (Eds.), The Great American Carbonate Bank: The Geology and Economic Resources of the Cambrian–Ordovician Sauk Megasequence of Laurentia. Association of American Petroleum Geologists Memoir 98, pp. 345–356.
Edwards, C.T., Saltzman, M.R., 2014. Carbon isotope (delta C-13(carb)) stratigraphy of the Lower–Middle Ordovician (Tremadocian–Darriwilian) in the Great Basin, western United States: implications for global correlation. Palaeogeogr. Palaeoclimatol. Palaeoecol. 399, 1–20.
Edwards, C.T., Saltzman, M.R., 2016. Paired carbon isotopic analysis of Ordovician bulk carbonate (d^{13}Ccarb) and organic matter (d^{13}Corg) spanning the Great Ordovician Biodiversification Event. Palaeogeogr. Palaeoclimatol. Palaeoecol. 458, 102–117.
Edwards, C.T., Saltzman, M.R., Leslie, S.A., Bergstrom, S.M., Sedlacek, A.R.C., Howard, A., Bauer, J.A., Sweet, W.C., Young, S.A., 2015. Strontium isotope (87Sr/86Sr) stratigraphy of Ordovician bulk carbonate: implications for preservation of primary seawater values. Geol. Soc. Am. Bull. 127 (9–10), 1275–1289.
Fike, D.A., Grotzinger, J.P., Pratt, L.M., Summons, R.E., 2006. Oxidation of the Ediacaran Ocean. Nature 444 (7120), 744–747.
Finney, S.C., Ethington, R.L., Repetski, J.E., 2007. The boundary between the Sauk and Tippecanoe Sloss sequences in North America Acta Palaeontologica Sinica. vol. 46 pp. 128–134.
Frakes, L.A., Francis, J.E., Syktus, J.I., 1992. Climate Modes of the Phanerozoic. Cambridge University Press, Cambridge (274 pp.).
Fry, B., Jannasch, H.W., Molyneaux, S.J., Wirsen, C.O., Muramoto, J.A., King, S., 1991. Stable isotope studies of the carbon, nitrogen and sulfur cycles in the Black-Sea and the Cariaco Trench. Deep Sea Res. Part A 38, S1003–S1019.
Garrels, R.M., Lerman, A., 1981. Phanerozoic cycles of sedimentary carbon and sulfur. Proc. Natl. Acad. Sci. U. S. A.-Phys. Sci. 78 (8), 4652–4656.
Garrels, R.M., Lerman, A., 1984. Coupling of the sedimentary sulfur and carbon cycles — an improved model. Am. J. Sci. 284 (9), 989–1007.
Gill, B.C., Lyons, T.W., Saltzman, M.R., 2007. Parallel, high-resolution carbon and sulfur isotope records of the evolving Paleozoic marine sulfur reservoir. Palaeogeogr. Palaeoclimatol. Palaeoecol. 256 (3–4), 156–173.
Gill, B.C., Lyons, T.W., Frank, T.D., 2008. Behavior of carbonate-associated sulfate during meteoric diagenesis and implications for the sulfur isotope paleoproxy. Geochim. Cosmochim. Acta 72 (19), 4699–4711.
Gill, B.C., Lyons, T.W., Jenkyns, H.C., 2011a. A global perturbation to the sulfur cycle during the Toarcian Oceanic Anoxic Event. Earth Planet. Sci. Lett. 312 (3–4), 484–496.
Gill, B.C., Lyons, T.W., Young, S.A., Kump, L.R., Knoll, A.H., Saltzman, M.R., 2011b. Geochemical evidence for widespread euxinia in the Later Cambrian ocean. Nature 469 (7328), 80–83.
Given, R.K., Lohmann, K.C., 1986. Isotopic evidence for the early meteoric diagenesis of the reef facies Permian Reef Complex of West Texas and New-Mexico. J. Sediment. Petrol. 56 (2), 183–193.
Gleason, J.D., Finney, S.C., Gehrels, G.E., 2002. Paleotectonic implications of a mid- to late-Ordovician provenance shift, as recorded in sedimentary strata of the ouachita and southern Appalachian mountains. J. Geol. 110 (3), 291–304.
Goldhaber, M.B., Kaplan, I.R., 1975. Controls and consequences of sulfate reduction rates in recent marine sediments. Soil Sci. 119 (1), 42–55.
Gomes, M.L., Hurtgen, M.T., 2013. Sulfur isotope systematics of a euxinic, low-sulfate lake: evaluating the importance of the reservoir effect in modern and ancient oceans. Geology 41 (6), 663–666.
Gomes, M.L., Hurtgen, M.T., 2015. Sulfur isotope fractionation in modern euxinic systems: implications for paleoenvironmental reconstructions of paired sulfate–sulfide isotope records. Geochim. Cosmochim. Acta 157, 39–55.
Habicht, K.S., Canfield, D.E., 1996. Sulphur isotope fractionation in modern microbial mats and the evolution of the sulphur cycle. Nature 382 (6589), 342–343.
Habicht, K.S., Canfield, D.E., 2001. Isotope fractionation by sulfate-reducing natural populations and the isotopic composition of sulfide in marine sediments. Geology 29 (6), 555–558.
Habicht, K.S., Canfield, D.E., Rethmeier, J., 1998. Sulfur isotope fractionation during bacterial reduction and disproportionation of thiosulfate and sulfite. Geochim. Cosmochim. Acta 62 (15), 2585–2595.
Habicht, K.S., Gade, M., Thamdrup, B., Berg, P., Canfield, D.E., 2002. Calibration of sulfate levels in the. Archean Ocean: Science 298 (5602), 2372–2374.
Halverson, G.P., Hurtgen, M.T., 2007. Ediacaran growth of the marine sulfate reservoir. Earth Planet. Sci. Lett. 263 (1–2), 32–44.
Ham, W.E., 1969. Regional geology of the Arbuckle Mountains, Oklahoma. Oklahoma Geological Survey Guidebook 17 p. 52.
Hammarlund, E.U., Dahl, T.W., Harper, D.A.T., Bond, D.P.G., Nielsen, A.T., Bjerrum, C.J., Schovsbo, N.H., Schonlaub, H.P., Zalasiewicz, J.A., Canfield, D.E., 2012. A sulfidic driver for the end-Ordovician mass extinction. Earth Planet. Sci. Lett. 331, 128–139.
Harper, D.A.T., 2006. The Ordovician biodiversification: setting an agenda for marine life. Palaeogeogr. Palaeoclimatol. Palaeoecol. 232 (2–4), 148–166.
Harrison, A.G., Thode, H.G., 1958. Mechanism of the bacterial reduction of sulphate from isotope fractionation studies. Trans. Faraday Soc. 54 (1), 84–92.
Hoffman, P.F., Dewey, J.F., Burke, K.C., 1974. Aulacogens and Their Genetic Relation to Geosynclines, with a Proterozoic Example from Great Slave Lake, Canada. In: Dott, R.H.J., Shaver, R.H. (Eds.), Modern ancient geosynclinal sedimentation Society of Economic Paleontologists and Mineralogists. Special Publication 19, pp. 38–55.
Holser, W.T., Schidlowski, M., Mackenzie, F.T., Maynard, J.B., 1988. Geochemical cycles of carbon and sulfur. In: Garrels, R.M., Mackenzie, F.T., Maynard, J.B., Gregor, C.B. (Eds.), Chemical Cycles in the Evolution of Earth. Wiley, New York, pp. 105–173.
Horita, J., Zimmermann, H., Holland, H.D., 2002. Chemical evolution of seawater during the Phanerozoic: implications from the record of marine evaporites. Geochim. Cosmochim. Acta 66 (21), 3733–3756.
Hough, M.L., Shields, G.A., Evins, L.Z., Strauss, H., Henderson, R.A., Mackenzie, S., 2006. A major sulphur isotope event at c.510 Ma: a possible anoxia–extinction–volcanism connection during the Early–Middle Cambrian transition? Terra Nova 18 (4), 257–263.
Hurtgen, M.T., Halverson, G.P., Arthur, M.A., Hoffman, P.F., 2006. Sulfur cycling in the aftermath of a 635-Ma snowball glaciation: evidence for a syn-glacial sulfidic deep ocean. Earth Planet. Sci. Lett. 245 (3–4), 551–570.
Hurtgen, M.T., Pruss, S.B., Knoll, A.H., 2009. Evaluating the relationship between the carbon and sulfur cycles in the later Cambrian ocean: an example from the Port au Port Group, western Newfoundland, Canada. Earth Planet. Sci. Lett. 281 (3–4), 288–297.
Husinec, A., Bergström, S.M., 2015. Stable carbon-isotope record of shallow-marine evaporative epicratonic basin carbonates, Ordovician Williston Basin, North America. Sedimentology 62, 314–349.
Ingram, B.L., Coccioni, R., Montanari, A., Richter, F.M., 1994. Strontium isotopic composition of midcretaceous seawater. Science 264 (5158), 546–550.
John, E.H., Wignall, P.B., Newton, R.J., Bottrell, S.H., 2010. δ34SCASand δ18OCAS records during the Frasnian–Famennian (Late Devonian) transition and their bearing on mass extinction models. Chem. Geol. 275, 221–234.
Jones, D.S., Fike, D.A., 2013. Dynamic sulfur and carbon cycling through the end-Ordovician extinction revealed by paired sulfate-pyrite delta S-34. Earth Planet. Sci. Lett. 363, 144–155.
Jones, C.E., Jenkyns, H.C., 2001. Seawater strontium isotopes, oceanic anoxic events, and seafloor hydrothermal activity in the Jurassic and Cretaceous. Am. J. Sci. 301 (2), 112–149.
Jones, C.E., Jenkyns, H.C., Coe, A.L., Hesselbo, S.P., 1994. Strontium isotopic variations in Jurassic and cretaceous seawater. Geochim. Cosmochim. Acta 58 (14), 3061–3074.
Kah, L.C., Lyons, T.W., Frank, T.D., 2004. Low marine sulphate and protracted oxygenation of the proterozoic biosphere. Nature 431 (7010), 834–838.
Kampschulte, A., Bruckschen, P., Strauss, H., 2001. The sulphur isotopic composition of trace sulphates in Carboniferous brachiopods: implications for coeval seawater, correlation with other geochemical cycles and isotope stratigraphy. Chem. Geol. 175 (1–2), 149–173.
Kanyigan, A.V., Koren, T.N., Yadrenkina, A.G., Timokhin, A.V., Sychev, O.V., Tolmacheva, T.Y., 2010. Ordovician of Siberian Platform. In: Finney, S.C., Berry, W.B.N. (Eds.), The Ordovician Earth System. Geological Society of America Special Paper 466, pp. 105–118.
Kaplan, I.R., Rittenberg, S.C., 1964. Microbiological fractionation of sulphur isotopes. J. Gen. Microbiol. 34 (2), 195–212.
Kaufman, A.J., Hayes, J.M., Knoll, A.H., Germs, G.J.B., 1991. Isotopic compositions of carbonates and organic-carbon from Upper Proterozoic successions in Namibia — stratigraphic variation and the effects of diagenesis and metamorphism. Precambrian Res. 49 (3–4), 301–327.
Kump, L.R., 1989. Alternative modeling approaches to the geochemical cycles of carbon sulfur, and strontium isotopes. Am. J. Sci. 289 (4), 390–410.
Kump, L.R., Arthur, M.A., 1999. Interpreting carbon–isotope excursions: carbonates and organic matter. Chem. Geol. 161 (1–3), 181–198.
Kump, L.R., Garrels, R.M., 1986. Modeling atmospheric O-2 in the global sedimentary redox cycle. Am. J. Sci. 286 (5), 337–360.
Kump, L.R., Arthur, M.A., Patzkowsky, M.E., Gibbs, M.T., Pinkus, D.S., Sheehan, P.M., 1999. A weathering hypothesis for glaciation at high atmospheric pCO(2) during the Late Ordovician. Palaeogeogr. Palaeoclimatol. Palaeoecol. 152 (1–2), 173–187.
Kurtz, A.C., Kump, L.R., Arthur, M.A., Zachos, J.C., Paytan, A., 2003. Early Cenozoic decoupling of the global carbon and sulfur cycles. Paleoceanography 18 (4).
Lasaga, A.C., 1980. The kinetic treatment of geochemical cycles. Geochim. Cosmochim. Acta 44, 815–828.
Lasaga, A.C., Berner, R.A., 1998. Fundamental aspects of quantitative models for geochemical cycles. Chem. Geol. 145, 161–175.
Leavitt, W.D., Halevy, I., Bradley, A.S., Johnston, D.T., 2013. Influence of sulfate reduction rates on the Phanerozoic sulfur isotope record. Proc. Natl. Acad. Sci. U. S. A. 110 (28), 11244–11249.

Lefticariu, L., Pratt, L.M., Ripley, E.M., 2006. Mineralogic and sulfur isotopic effects accompanying oxidation of pyrite in millimolar solutions of hydrogen peroxide at temperatures from 4 to 150 °C. Geochim. Cosmochim. Acta 70 (19), 4889–4905.
Lenton, T.M., Watson, A.J., 2000. Redfield revisited: 2. What regulates the oxygen content of the atmosphere? Glob. Biogeochem. Cycles 14 (1), 249–268.
Leslie, S.A., Saltzman, M.R., Bergström, S.M., Repetski, J.E., Howard, A., Seward, A.M., 2011. Conodont biostratigraphy and stable isotope stratigraphy across the Knox/Beekmantown unconformity in the Central Appalachians. In: Gutierrez-Marco, J.C., Rabano, I., Garcia-Bellido, D. (Eds.), Ordovician of the World vol. 14. Caudernos del Museo Geominero, pp. 301–308.
Leslie, S.A., Repetski, J.E., Saltzman, M.R., Kaznosky, C.M., Lizer, A.M., 2013. Conodont biostratigraphy of the Rockdale Run Formation, Pinesburg Station Dolomite, St. Paul Group, and Chambersburg Formation (Middle to Lower Upper Ordovician) near Clear Spring, Maryland. Denver, Colorado, Geological Society of America Abstracts with Programs 45 p. 836.
Lewis, R.D., 1982. Depositional Environments and Paleoecology of the Oil Creek Formation (Middle Ordovician), Arbuckle Mountains and Criner Hills, Oklahoma (Ph.D. Dissertation), University of Texas (352 pp.).
Li, C., Love, G.D., Lyons, T.W., Fike, D.A., Sessions, A.L., Chu, X.L., 2010. A stratified redox model for the Ediacaran Ocean. Science 328 (5974), 80–83.
Longman, M.W., Fertal, T.G., Glennie, J.S., 1983. Origin and geometry of Red River Dolomite Reservoirs, Western Williston Basin. Bull. Am. Assoc. Pet. Geol. 67 (5), 744–771.
Lowenstein, T.K., Timofeeff, M.N., Kovalevych, V.M., Horita, J., 2005. The major-ion composition of Permian seawater. Geochim. Cosmochim. Acta 69 (7), 1701–1719.
Lyons, T.W., Walter, L.M., Gellatly, A.M., Martini, A.M., Blake, R.E., 2004. Sites of anomolous organic remineralization in the carbonate sediments of South Florida, USA: the sulfur cycle and carbonate-associated sulfate. In: Amend, J.P., Edwards, K.J., Lyons, T.W. (Eds.), Sulfur Biogeochemistry Past and Present: Geological Society of America Special Paper 379, pp. 161–178.
Lyons, T.W., Anbar, A.D., Severmann, S., Scott, C., Gill, B.C., 2009. Tracking Euxinia in the Ancient Ocean: a multiproxy perspective and Proterozoic case study. Annu. Rev. Earth Planet. Sci. 37, 507–534.
Marenco, P.J., Corsetti, F.A., Hammond, D.E., Kaufman, A.J., Bottjer, D.J., 2008a. Oxidation of pyrite during extraction of carbonate associated sulfate. Chem. Geol. 247 (1–2), 124–132.
Marenco, P., Corsetti, F.A., Kaufman, A.J., Bottjer, D.J., 2008b. Environmental and diagenetic variations in carbonate associated sulfate: an investigation of CAS in the Lower Triassic of the western USA. Geochim. Cosmochim. Acta 72, 1570–1582.
Marenco, P.J., Marenco, K.N., Lubitz, R.L., Niu, D., 2013. Contrasting longterm global and short-term local redox proxies during the Great Ordovician Biodiversification Event: a case study from Fossil Mountain, Utah, USA. Palaeogeogr. Palaeoclimatol. Palaeoecol. 377, 45–51. http://dx.doi.org/10.1016/j.palaeo.2013.03.007.
McArthur, J.M., Howarth, R.J., Bailey, T.R., 2001. Strontium isotope stratigraphy: LOWESS version 3: best fit to the marine Sr-isotope curve for 0–509 Ma and accompanying look-up table for deriving numerical age. J. Geol. 109 (2), 155–170.
McArthur, J.M., Howarth, R.J., Shields, G.A., 2012. Strontium isotope stratigraphy. In: Gradstein, F.M., Ogg, J.G., Schimtz, M.D., Ogg, G.M. (Eds.), The Geologic Time Scale. Elsevier, Amsterdam, pp. 127–144.
Miller, A.I., Mao, S.G., 1995. Association of orogenic activity with the Ordovician radiation of marine life. Geology 23 (4), 305–308.
Mitchell, R.W., 1985. Comparative sedimentology of shelf carbonates of the Middle Ordovician St-Paul Group, Central Appalachians. Sediment. Geol. 43 (1–4), 1–41.
Munnecke, A., Zhang, Y.D., Liu, X., Cheng, J.F., 2011. Stable carbon isotope stratigraphy in the Ordovician of South China. Palaeogeogr. Palaeoclimatol. Palaeoecol. 307 (1–4), 17–43.
Murray, T.E., 1995. The correlation between iron sulfide precipitation and hypolimnetic phosphorus accumulation during one summer in a softwater lake. Can. J. Fish. Aquat. Sci. 52, 1190–1194.
Mussman, W.J., Read, J.F., 1986. Sedimentology and development of a passive-margin to convergent-margin unconformity — Middle Ordovician Knox Unconformity Virginia Appalachians. Geol. Soc. Am. Bull. 97 (3), 282–295.
Nielsen, A.T., 2004. Ordovician sea level changes: a Baltoscandian perspective. In: Paris, F., Droser, M.L., Percival, I.G., Webby, B.D. (Eds.), The Great Ordovician Biodiversification Event. Columbia University Press, New York, pp. 84–96.
Paytan, A., Kastner, M., Campbell, D., Thiemens, M.H., 2004. Seawater sulfur isotope fluctuations in the cretaceous. Science 304 (5677), 1663–1665.
Peng, Y.B., Bao, H.M., Pratt, L.M., Kaufman, A.J., Jiang, G.Q., Boyd, D., Wang, Q.X., Zhou, C.M., Yuan, X.L., Xiao, S.H., Loyd, S., 2014. Widespread contamination of carbonate-associated sulfate by present-day secondary atmospheric sulfate: evidence from triple oxygen isotopes. Geology 42 (9), 815–818.
Pruss, S.B., Finnegan, S., Fischer, W.W., Knoll, A.H., 2010. Carbonates in skeleton-poor seas: new insights from Cambrian and Ordovician strata of Laurentia. Palaios 25, 73–84. http://dx.doi.org/10.2110/palo.2009.p09-101r.
Qing, H.R., Barnes, C.R., Buhl, D., Veizer, J., 1998. The strontium isotopic composition of Ordovician and Silurian brachiopods and conodonts: relationships to geological events and implications for coeval seawater. Geochim. Cosmochim. Acta 62 (10), 1721–1733.
Raab, M., Spiro, B., 1991. Sulfur isotopic variations during seawater evaporation with fractional crystallization. Chem. Geol. 86 (4), 323–333.
Rasmussen, C.M.Ø., Hansen, J., Harper, D.A.T., 2007. Baltica: a mid Ordovician diversity hotspot. Historical Biology vol. 19 pp. 255–261.
Read, J.F., Repetski, J.E., 2012. Cambrian–Lower Middle Ordovician passive carbonate margin, southern Appalachians. In: Derby, J.R., Fritz, R.D., Longacre, S.A., Morgan, W.A., Sternbach, C.A. (Eds.), The Great American Carbonate Bank: The Geology and Economic Resources of the Cambrian–Ordovician Sauk Megasequence of Laurentia. Association of American Petroleum Geologists Memoir 98, pp. 357–382.
Repetski, J.E., Harris, A.G., 1986. Conodont biostratigraphy and biofacies of Upper Knox Beekmantown Groups and overlying Ordovician rocks in Appalachian Basin, New-York to Alabama. Bull. Am. Assoc. Pet. Geol. 70 (5), 637–638.
Ries, J.B., Fike, D.A., Pratt, L.M., Lyons, T.W., Grotzinger, J.P., 2009. Superheavy pyrite (delta S-34(pyr) > delta S-34(CAS)) in the terminal Proterozoic Nama Group, Southern Namibia: a consequence of low seawater sulfate at the dawn of animal life. Geology 37 (8), 743–746.
Sælen, G., Raiswell, R., Talbot, M.R., Skei, J.M., Bottrell, S.H., 1993. Heavy sedimentary sulfur isotopes as indicators of super-anoxic bottom-water conditions. Geology 21, 1091–1094.
Saltzman, M.R., 2005. Phosphorus, nitrogen, and the redox evolution of the Paleozoic oceans. Geology 33 (7), 573–576.
Saltzman, M.R., Ripperdan, R.L., Brasier, M.D., Lohmann, K.C., Robison, R.A., Chang, W.T., Peng, S.C., Ergaliev, E.K., Runnegar, B., 2000. A global carbon isotope excursion (SPICE) during the Late Cambrian: relation to trilobite extinctions, organic-matter burial and sea level. Palaeogeogr. Palaeoclimatol. Palaeoecol. 162 (3–4), 211–223.
Saltzman, M.R., Groessens, E., Zhuravlev, A.V., 2004. Carbon cycle models based on extreme changes in delta C-13: an example from the lower Mississippian. Palaeogeogr. Palaeoclimatol. Palaeoecol. 213 (3–4), 359–377.
Saltzman, M.R., Young, S.A., Kump, L.R., Gill, B.C., Lyons, T.W., Runnegar, B., 2011. Pulse of atmospheric oxygen during the late Cambrian. Proc. Natl. Acad. Sci. U. S. A. 108 (10), 3876–3881.
Saltzman, M.R., Edwards, C.T., Leslie, S.A., Dwyer, G.S., Bauer, J.A., Repetski, J.E., Harris, A.G., Bergstrom, S.M., 2014. Calibration of a conodont apatite-based Ordovician Sr-87/Sr-86 curve to biostratigraphy and geochronology: implications for stratigraphic resolution. Geol. Soc. Am. Bull. 126 (11–12), 1551–1568.
Saltzman, M.R., Edwards, C.T., Adrain, J.M., Westrop, S.R., 2015. Persistent oceanic anoxia and elevated extinction rates separate the Cambrian and Ordovician radiations. Geology 43, 807–810. http://dx.doi.org/10.1130/G36814.1.
Schmitz, B., Harper, D.A.T., Peucker-Ehrenbrink, B., Stouge, S., Alwmark, C., Cronholm, A., Bergstrom, S.M., Tassinari, M., Xiaofeng, W.F., 2008. Asteroid breakup linked to the Great Ordovician Biodiversification Event. Nat. Geosci. 1 (1), 49–53.
Schmitz, B., Bergstroem, S.M., Wang, X.F., 2010. The middle Darriwilian (Ordovician) delta(13)C excursion (MDICE) discovered in the Yangtze Platform succession in China: implications of its first recorded occurrences outside Baltoscandia. J. Geol. Soc. 167 (2), 249–259.
Sepkoski, J.J., Bambach, R.K., Raup, D.M., Valentine, J.W., 1981. Phanerozoic marine diversity and the fossil record. Nature 293 (5832), 435–437.
Servais, T., Lehnert, O., Li, J., Mullins, G.L., Munnecke, A., Nutzel, A., Vecoli, M., 2008. The Ordovician Biodiversification: revolution in the oceanic trophic chain. Lethaia 41 (2), 99–109.
Servais, T., Owen, A.W., Harper, D.A.T., Kroger, B., Munnecke, A., 2010. The Great Ordovician Biodiversification Event (GOBE): the palaeoecological dimension. Palaeogeogr. Palaeoclimatol. Palaeoecol. 294 (3–4), 99–119.
Sheehan, P.M., 2001. The Late Ordovician mass extinction. Annu. Rev. Earth Planet. Sci. 29, 331–364.
Shen, B., Mao, S.H., Kaufman, A.J., Bao, H.M., Zhou, C.M., Wang, H.F., 2008. Stratification and mixing of a post-glacial Neoproterozoic ocean: evidence from carbon and sulfur isotopes in a cap dolostone from northwest China. Earth Planet. Sci. Lett. 265 (1–2), 209–228.
Shields, G.A., Carden, G.A.F., Veizer, J., Meidla, T., Rong, J.Y., Li, R.Y., 2003. Sr C, and O isotope geochemistry of Ordovician brachiopods: a major isotopic event around the Middle–Late Ordovician transition. Geochim. Cosmochim. Acta 67 (11), 2005–2025.
Sim, M.S., Bosak, T., Ono, S., 2011a. Large sulfur isotope fractionation does not require disproportionation. Science 333 (6038), 74–77.
Sim, M.S., Ono, S., Donovan, K., Templer, S.P., Bosak, T., 2011b. Effect of electron donors on the fractionation of sulfur isotopes by a marine *Desulfovibrio* sp. Geochim. Cosmochim. Acta 75 (15), 4244–4259.
Sim, M.S., Ono, S.H., Hurtgen, M.T., 2015. Sulfur isotope evidence for low and fluctuating sulfate levels in the Late Devonian ocean and the potential link with the mass extinction event. Earth Planet. Sci. Lett. 419, 52–62.
Sperling, E.A., Wolock, C.J., Morgan, A.S., Gill, B.C., Kunzmann, M., Halverson, G.P., Mcdonald, F.A., Knoll, A.H., Johnston, D.T., 2015. Statistical analysis of iron geochemical data suggests limited late Proterozoic oxygenation. Nature 523, 451–454.
Steemans, P., Wellman, C.H., 2004. Miospores and the emergence of land plants. In: Paris, F., Droser, M.L., Percival, I.G., Webby, B.D. (Eds.), The Great Ordovician Biodiversification Event. Columbia University Press, New York, pp. 361–368.
Stouge, S.S., 1984. Conodonts from the Middle Ordovician Table Head Formation, Western Newfoundland. Fossils Strata 16, 1–145.
Thode, H.G., Monster, J., Dunford, H.B., 1961. Sulphur isotope geochemistry. Geochim. Cosmochim. Acta 25 (3), 159–174.
Thompson, C.K., Kah, L.C., 2012. Sulfur isotope evidence for widespread euxinia and a fluctuating oxycline in Early to Middle Ordovician greenhouse oceans. Palaeogeogr. Palaeoclimatol. Palaeoecol. 313, 189–214.
Trotter, J.A., Williams, I.S., Barnes, C.R., Lecuyer, C., Nicoll, R.S., 2008. Did cooling oceans trigger Ordovician biodiversification? Evidence from conodont thermometry. Science 321 (5888), 550–554.
Webby, B.D., Droser, M.L., Paris, F., Percival, I.G., 2004. The Great Ordovician Biodiversification Event. Columbia University Press, New York (484 pp.).
Williams, G.E., 1991. Milankovitch-Band cyclicity in bedded halite deposits contemporaneous with Late Ordovician–Early Silurian glaciation, Canning Basin, Western Australia. Earth Planet. Sci. Lett. 103 (1–4), 143–155.
Wortmann, U.G., Chernyavsky, B.M., 2007. Effect of evaporite deposition on Early Cretaceous carbon and sulphur cycling. Nature 446 (7136), 654–656.
Wortmann, U.G., Paytan, A., 2012. Rapid variability of seawater chemistry over the past 130 million years. Science 337 (6092), 334–336.

Wotte, T., Shields-Zhou, G.A., Strauss, H., 2012. Carbonate-associated sulfate: experimental comparisons of common extraction methods and recommendations toward a standard analytical protocol. Chem. Geol. 326, 132–144.
Yan, D.T., Chen, D.Z., Wang, Q.C., Wang, J.G., Wang, Z.Z., 2009. Carbon and sulfur isotopic anomalies across the Ordovician–Silurian boundary on the Yangtze Platform, South China. Palaeogeogr. Palaeoclimatol. Palaeoecol. 274 (1–2), 32–39.
Young, S.A., Saltzman, M.R., Bergstrom, S.M., Leslie, S.A., Xu, C., 2008. Paired delta C-13(carb) and delta C-13(org) records of Upper Ordovician (Sandbian–Katian) carbonates in North America and China: implications for paleoceanographic change. Palaeogeogr. Palaeoclimatol. Palaeoecol. 270 (1–2), 166–178.
Young, S.A., Saltzman, M.R., Foland, K.A., Linder, J.S., Kump, L.R., 2009. A major drop in seawater Sr-87/Sr-86 during the Middle Ordovician (Darriwilian): links to volcanism and climate? Geology 37 (10), 951–954.
Zhan, R., Harper, D.A.T., 2006. Biotic diachroneity during the Ordovician radiation: evidence from South China. Lethaia 39 (3), 211–226.